SRNL-STI-2011-00441

Key Words:
Grout Stirring, CFD, Agitator

Retention:
Permanent

GROUT HOPPER MODELING STUDY

JULY 2011

Savannah River National Laboratory
Savannah River Nuclear Solutions
Aiken, SC 29808

Prepared for the U.S. Department of Energy Under Contract Number DE-AC09-08SR22470

DISCLAIMER

Printed in the United States of America

Prepared for
U.S. Department of Energy

SRNL-STI-2011-00441

Key Words:
Grout Stirring, CFD,
Agitator

Retention:
Permanent

GROUT HOPPER MODELING STUDY

Si Y. Lee
Jason M. Ryans*
*2011 Summer Intern
(Mercer University)

JULY 2011

Savannah River National Laboratory
Savannah River Nuclear Solutions
Savannah River Site
Aiken, SC 29808

Prepared for the U.S. Department of Energy Under
Contract Number DE-AC09-08SR22470

TABLE OF CONTENTS

LIST OF FIGURES

LIST OF TABLES

NOMENCLATURE

A	Area
C_μ	Turbulent viscosity coefficient
D	Tank diameter
D_B	Blade diameter
g	Gravitational acceleration
H_c	Critical height to prevent air entrainment to the blade
k	Kinetic energy
k	Kinetic energy
N	Speed of agitator rotation (revolutions per unit time)
P	Turbulent production rate or power consumption
p	Pressure
Δp	Pressure drop
Q	Volumetric flow rate
U	Maximum downward velocity
u	Local velocity along the x-axis
v	Local velocity along the y-axis
w	Local velocity along the z-axis
x	Local distance along the x-axis
y	Local distance along the y-axis
z	Local distance along the z-axis
ρ_f	Fluid density
ρ_a	Air density
ν	Kinematic viscosity
τ	Shear stress
κ	Turbulent kinetic energy per unit mass
ε	Turbulent energy dissipation rate per unit mass
τ_o	Yield stress
T'	Turbulent energy transport
σ_k	Turbulent Prandtl number
η_∞	Plastic viscosity or consistency
$\dot{\gamma}$	Shear rate
μ	Dynamic viscosity
in	Inch (=0.0254 m)
Fr	Froude number
Re	Reynolds number
CFD	Computational Fluid Dynamics
DOE	United States Department of Energy
FLUENT	CFD software code
SRS	Savannah River Site
SWPF	Salt Waste Processing Facility

1.0 ABSTRACT

The Saltstone facility has a grout hopper tank to provide agitator stirring of the Saltstone feed materials. The tank has about 300 gallon capacity to provide a larger working volume for the grout slurry to be held in case of a process upset, and it is equipped with a mechanical agitator, which is intended to keep the grout in motion and agitated so that it won't start to set up. The dry feeds and the salt solution are already mixed in the mixer prior to being transferred to the hopper tank. The hopper modeling study through this work will focus on fluid stirring and agitation, instead of traditional mixing in the literature, in order to keep the tank contents in motion during their residence time so that they will not be upset or solidified prior to transferring the grout to the Saltstone disposal facility.

The primary objective of the work is to evaluate the flow performance for mechanical agitators to prevent vortex pull-through for an adequate stirring of the feed materials and to estimate an agitator speed which provides acceptable flow performance with a 45^{o} pitched four-blade agitator. In addition, the power consumption required for the agitator operation was estimated.

The modeling calculations were performed by taking two steps of the Computational Fluid Dynamics (CFD) modeling approach. As a first step, a simple single-stage agitator model with 45^{o} pitched propeller blades was developed for the initial scoping analysis of the flow pattern behaviors for a range of different operating conditions. Based on the initial phase-1 results, the phase-2 model with a two-stage agitator was developed for the final performance evaluations.

A series of sensitivity calculations for different designs of agitators and operating conditions have been performed to investigate the impact of key parameters on the grout hydraulic performance in a 300-gallon hopper tank. For the analysis, viscous shear was modeled by using the Bingham plastic approximation. Steady state analyses with a two-equation turbulence model were performed with the FLUENT^{TM} codes. All analyses were based on three-dimensional results. Recommended operational guidance was developed by using the basic concept that local shear rate profiles and flow patterns can be used as a measure of hydraulic performance and spatial stirring. Flow patterns were estimated by a Lagrangian integration technique along the flow paths from the material feed inlet.

The modeling results show that when the two-stage agitator consisting of a 45^{o} pitched propeller and radial flat-plate blades is run at 140 rpm speed with 28 in diameter, the agitator provides an adequate stirring of the feed materials for a wide range of yield stresses (1 to 21 Pa) and the vortex system is shed into the remote region of the tank boundary by the blade passage in an efficient way. The results of this modeling study were used to develop the design guidelines for the agitator stirring and dispersion of the Saltstone feed materials in a hopper tank.

2.0 INTRODUCTION

The Saltstone facility has a grout hopper tank to provide agitator stirring of the Saltstone feed materials. The tank has about a 300 gallon capacity, and it is equipped with a mechanical agitator, which is intended to keep the grout in motion so that it won't start to set up. The dry feeds and the salt solution are already mixed in the mixer prior to being transferred to the hopper tank. The hopper system is being designed for an adequate stirring of the mixed feed materials without a vortex-type pull-through. The agitator modeling study through this work will focus on fluid stirring and agitation, instead of traditional mixing in the literature, in order to keep the hopper contents such as grout in motion so that they will not be upset or solidified prior to transferring the grout to the Saltstone disposal facility. The hopper mixing system equipped with a mechanical agitator is schematically shown in Fig. 1.

The Saltstone hopper modeling project is requesting a Computational Fluid Dynamics (CFD) modeling study from SRNL to evaluate the flow pattern behavior with a mechanical agitator and an estimate of the flow residence time in the grout hopper tank. The results of this study will be used to develop the design guidelines for the agitator stirring of the Saltstone feed materials. An analytical data validation package is not included in this task scope.

As requested by the customer, the objective of the present work is to:

- Evaluate the nominal agitator speed under the baseline conditions in terms of satisfying the acceptance flow criteria during the stirring operation in the hopper.
- Perform a sensitivity analysis with respect to the baseline design and operating conditions such as agitator speeds, fluid levels, and fluid properties.

The primary goal of the present work is to evaluate the flow stirring performance for mechanical agitators to prevent vortex pull-through and to estimate an agitator speed which provides acceptable flow performance with a 45^{o} pitched four-blade agitator. In addition, the power consumption will be estimated in a conservative way. The results of this modeling study will be used to develop the design guidelines for the agitator stirring of the Saltstone feed materials in a hopper tank.

For the modeling analysis, the flow patterns and shear rate profiles were primarily used as the performance acceptance criteria to allow adequate stirring prior to transfer of the hopper contents to the Saltstone processing facility. The criteria will avoid a vortex-type pull-through flow patterns with stagnation zones inside the hopper so that the feed materials will get stirred in a reasonable way, and also be prevented from being solidified in regions such as near the hopper wall boundary during the stirring process.

The present work for the hopper modeling study consists of two modeling stages. The 1^{st} stage modeling study was based on a single-stage agitator with four 45^{o} pitched flat-plate propeller blades for the initial phase-1 baseline analysis. The modeling domain and agitator geometry for the phase-1 study are shown in Figs. 1 and 2. Based on the initial phase-1 results, the phase-2 modeling study was based on a two-stage agitator for the improved performance calculations. The two-stage agitator is shown in Fig. 3. As shown in the figure, the upper agitator has the 45^{o} pitched propeller blades to promote the vertical fluid motion, and the lower one has the Rushton-type vertical blades to increase the fluid circulation in the radial direction. Each blade diameter for the phase-2 agitator is about two times larger than the phase-1 design to minimize the stagnation zone near the hopper wall boundary. The modeling conditions for the phase-1 and phase-2 modeling studies are provided in Table 1 and Table 2.

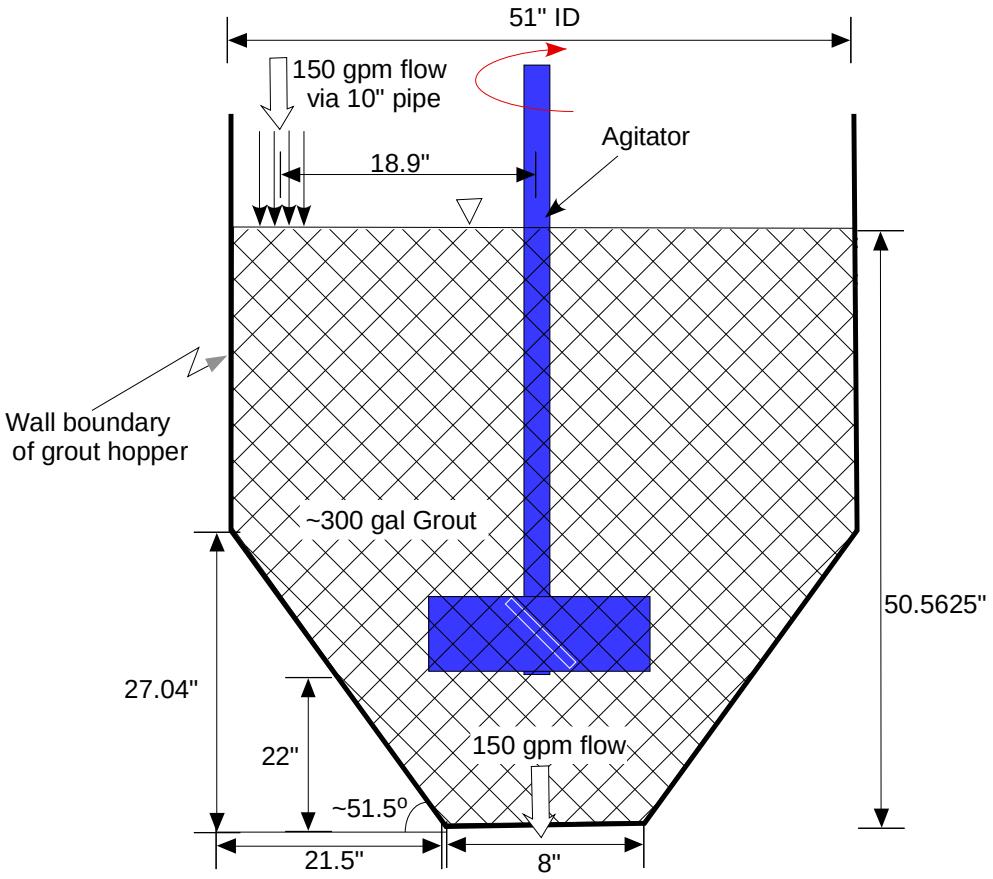

Figure 1. Geometry of the agitator tank with pitched blades used for the phase-1 baseline modeling analysis

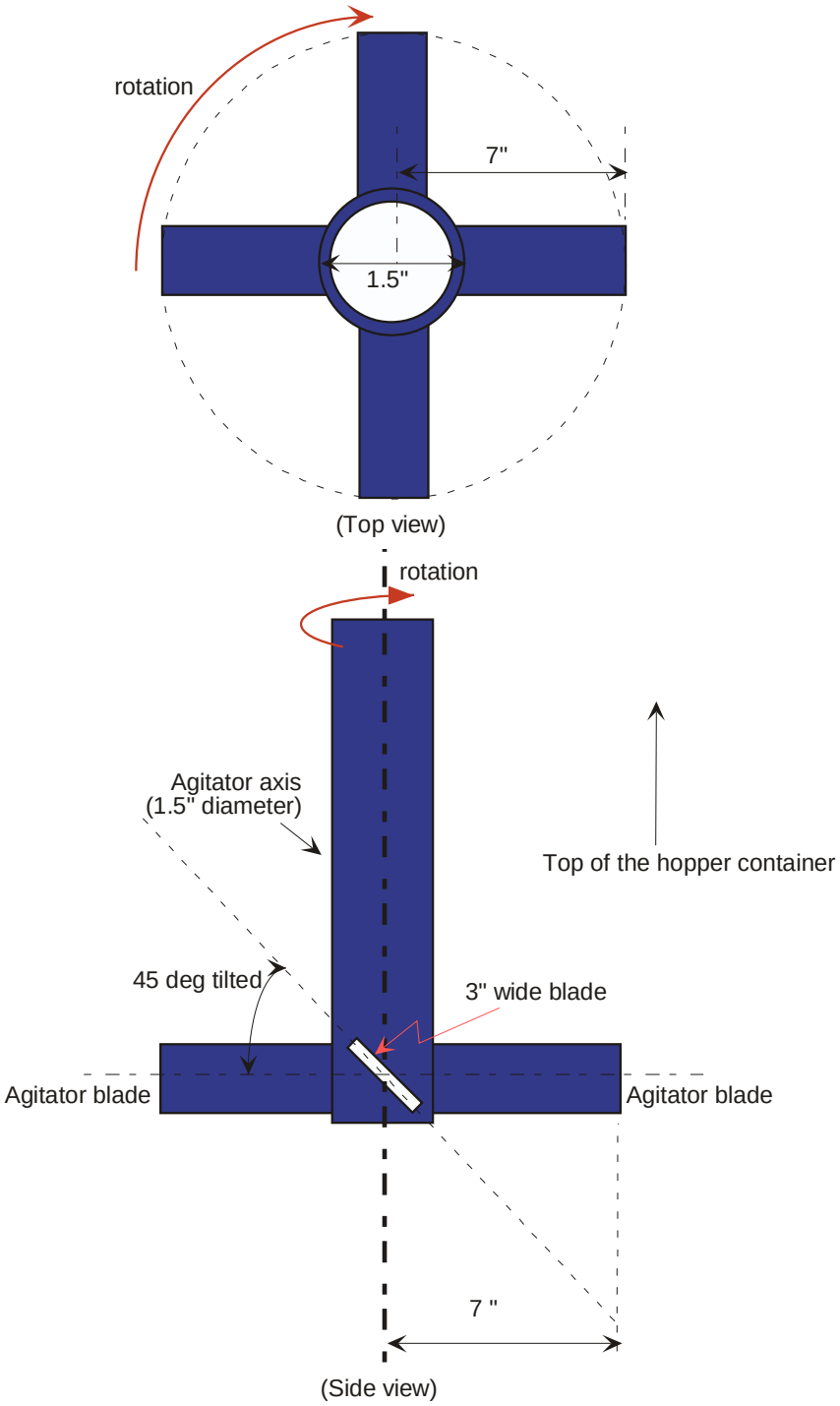

Figure 2. Configurations of the single-stage agitator with four 45^{o} pitched blades used for the phase-1 baseline model

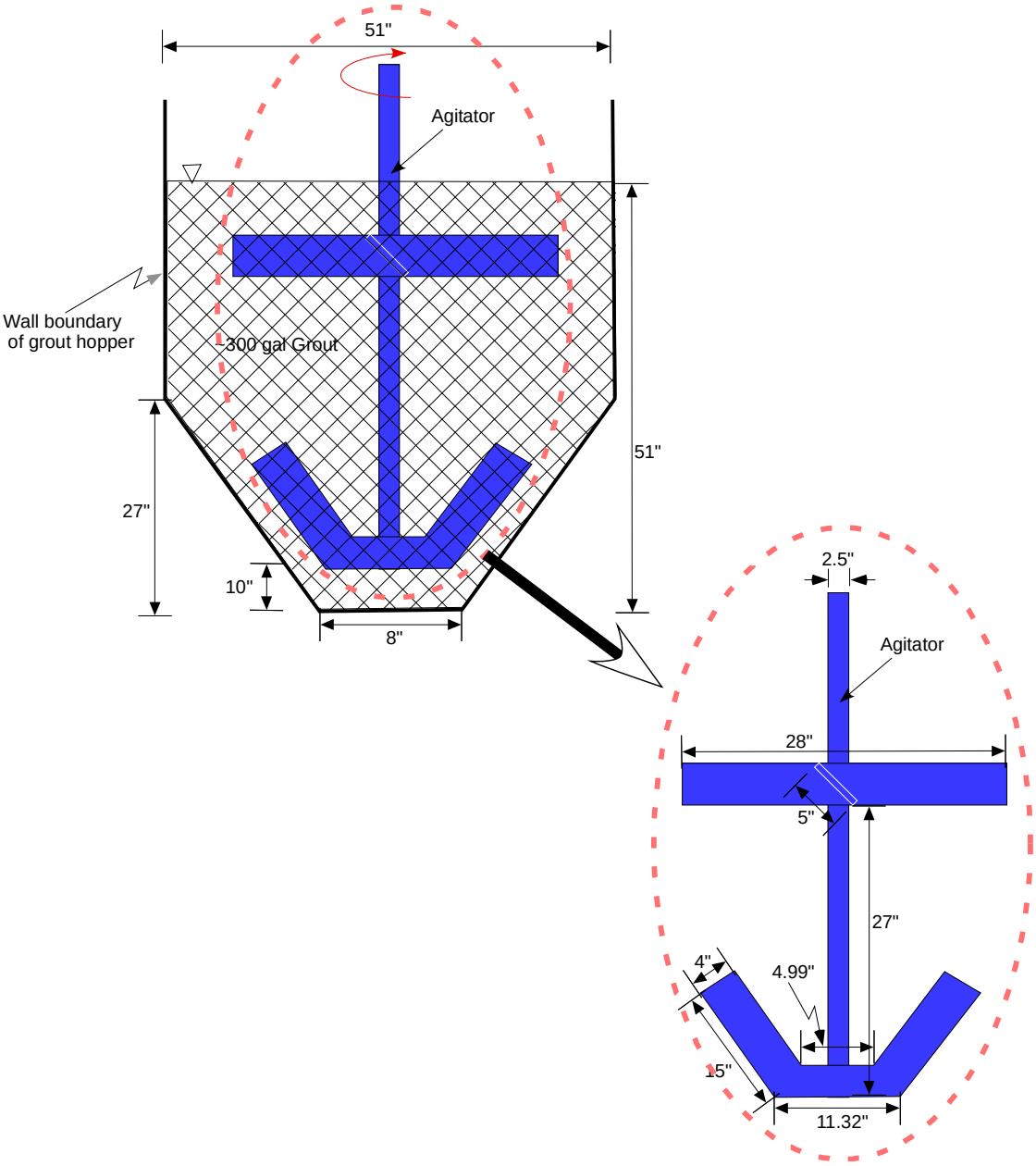

Figure 3. Geometry of the agitator tank with two-stage blades used for the phase-2 modeling analysis

Table 1. Baseline modeling conditions used for the initial phase-1 analysis

Parameters		Modeling conditions
Hopper dimensions and agitator geometry		See Figs. 1 and 2
Agitator blade shape and type		Four flat blade and propeller type
Steady-state flow rate to the hopper tank, gpm		150
Number of agitator stages		Single stage
Each blade dimension, inches		7” long, 3” wide
Tank fluid level, inches		51
Blade elevation from the tank bottom, inches		22
Nominal baseline operating conditions	Agitator speed, rpm	175 (641 ft/min. tip speed)
	Fluid consistency, cp	42
	Fluid specific gravity	1.75
	Fluid yield stress, Pa	0.01*, 1*, 10*, 21.546 (0.45 lb_f/ft^2)

Note:*For sensitivity analysis

Table 2. Modeling conditions used for the phase-2 performance analysis

Parameters		Modeling conditions
Hopper dimensions and agitator geometry		See Fig. 3
Agitator blade shape and type		Four blade and 45-deg propeller type for upper one, four radial blade for lower one
Steady-state flow rate to the hopper tank, gpm		150
Number of agitator stages		Two stage
Each blade dimension, inches		14” long, 5” wide for upper blade, 15” long, 4” wide for lower blade
Tank fluid level, inches		51
Blade elevation from the tank bottom, inches		10, 6*
Nominal baseline operating conditions	Agitator speed, rpm	69.3 (508 ft/min.), 140 (1026 ft/min)* 200 (1466 ft/min)*
	Fluid consistency, cp	42
	Fluid specific gravity	1.75
	Fluid yield stress, Pa	1*, 5, 21.546 (0.45 lbf/ft2)*

Note:* For sensitivity analysis

3.0 SOLUTION APPROACH AND MODELING ASSUMPTIONS

A three-dimensional CFD modeling method is used to achieve the objective. Based on the performance criteria discussed earlier, a steady-state computational approach was taken to compute flow fields driven by the agitator. The reference modeling conditions will be a 300-gallon hopper equipped with a four-blade flat propeller agitator with a 45^{o} angle for the initial phase-1 baseline calculations. The geometrical configurations for the modeling domain are shown in Figs. 1 and 2. The modeling simulations used three-dimensional steady-state, isothermal governing equations with multiple reference frames.

For the numerical modeling and calculations, three-dimensional steady-state momentum and continuity equations were used as the basic governing equations to estimate fluid motion driven by an agitator with four 45^{o} pitched blades. Hydraulic flow regime conditions were determined by estimating the Reynolds number corresponding to the operating conditions of a mechanical agitator considered for the Saltstone hopper modeling study. The laminar-turbulent transition occurred roughly around an impeller Reynolds number of 200 [Tatterson, 1991]. When the Reynolds number is larger than 200, a standard two-equation turbulence model, referred to as $\kappa-\varepsilon$ model in the literature, is used to capture turbulent eddy motion.

For incompressible steady-state flow, equation of the continuity is

$$\nabla \bullet \vec{v} = 0 \tag{1}$$

Equation of incompressible fluid motion is

$$\rho\left(\vec{v}\nabla\vec{v}\right) = -\nabla P + (\nabla \bullet \tau) + \rho\vec{g} \tag{2}$$

The shear force in Eq (2) term becomes

$$\left(\nabla \bullet \tau\right) = \mu \nabla \bullet \left(\nabla\vec{v}\right)$$

$$= \mu \nabla\left(\nabla \bullet \vec{v}\right) - \mu \nabla \times \left(\nabla \times \vec{v}\right)$$

$$= -\mu \nabla \times \vec{\Omega}$$

The resulting equation of incompressible steady-state motion is written as

$$\begin{aligned}\rho\left(\vec{v}\nabla\vec{v}\right) &= -\nabla P - \mu\nabla x\left(\nabla x\vec{v}\right) + \rho\vec{g} \\ &= -\nabla P - \mu\nabla x\vec{\Omega} + \rho\vec{g}\end{aligned} \tag{3}$$

Viscosity is the ability of a material to resist flow. Higher viscosity is characteristic of a less flowable suspension. The stress tensor can be expressed as

$$\bar{\tau} = -\bar{\eta}\left(\dot{\gamma}\right)\dot{\gamma} \tag{4}$$

where $\dot{\gamma} = \nabla v + \left(\nabla v\right)^T$ is the rate of strain tensor and the superscript *T* denotes matrix transpose.

The Herschel-Bulkley equation combines the Bingham and power-law models assuming viscosity to be independent of shear rate with zero-shear yield stress. The equation type is

$$\tau = \tau_o + k\dot{\gamma}^n \tag{5}$$

where τ_o and k in Eq. (5) are yield stress and consistency, respectively. When n is equal to 1, and the transition region is assumed to be negligible, Eq. (5) corresponds to the Bingham plastic model as shown in Fig. 2. As shown in the figure, consistency k becomes constant under the Bingham plastic model, that is, $k = \eta_\infty$.

$$\tau = \tau_o + \eta_\infty \dot{\gamma} \tag{6}$$

The transition region from shear-dependent viscosity to plastic viscosity of Newtonian fluid behavior was defined in implementing the Bingham plastic model in computational fluid dynamics approach as schematically shown in Fig. 2. As shown in the figure, plastic viscosity η_∞ is found from the slope of the linear portion of the curve. The yield stress τ_o, as identified in Fig. 2, is determined by extending the linear portion of the curve to the vertical coordinate axis. It is the minimum stress required for a material to start flowing and deforming.

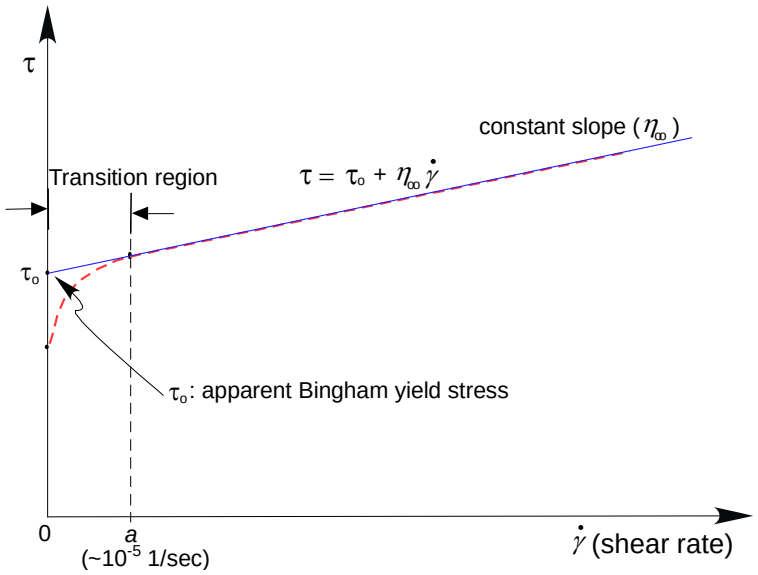

Figure 4. Bingham plastic model used in the present analysis

The analysis consists of two major parts. One part is to calculate the phase-1 operating conditions (single stage agitator and 175 rpm agitator speed) by applying the Bingham plastic model to the agitated fluid domain for the initial estimate of flow patterns and flow residence time. The operating conditions and agitator geometry for the phase-1 calculations are provided in Table 1 and Fig. 2. The second part is to apply the phase-1 methodology to the modeling simulations and flow pattern analysis of the phase-2 agitator for various yield stresses and agitator speeds to evaluate the stirring performance of the phase-2 two-stage agitator as shown in Fig. 3. As shown in Table 3 and Table 4, the initial scoping results show that the flow domain driven by the phase-1 agitator is laminar in terms of an agitator Reynolds number, while the phase-2 flow domain is turbulent.

Table 3. Flow conditions driven by the phase-1 baseline agitator shown in Fig. 2.

Pump speed		Agitator Reynolds number (Re_a)	Flow regime stirred by agitator
ft/min	rpm		
641	175**	~65	Laminar transition ($Re_a < 200$)
900	246	~90	

Note:* $Re_a = \left(\frac{\rho_f N D_B^{\ 2}}{\mu_f} \right)$, where N is the revolution of agitator per unit time.

** Nominal speed

Table 4. Flow conditions driven by the phase-2 two-stage agitator shown in Fig. 3.

Pump speed		Agitator Reynolds number (Re_a)	Flow regime stirred by agitator
ft/min	rpm		
508	69.3**	~205	Turbulent transition ($Re_a > 200$)
1026	140	~413	
1466	200	~590	

Note:* $Re_a = \left(\frac{\rho_f N D_B^{\,2}}{\mu_f} \right)$, where N and D_B are the revolution of agitator per unit time and blade diameter, respectively.

** Nominal speed

From two key turbulence parameters of k and ε, a quantity of turbulent eddy diffusivity (k^2/ε), can be formed without specification of flow-dependent mixing lengthscale λ [Jones and Launder, 1972]. When the turbulent energy transport term T' is modeled with a gradient-diffusion hypothesis as

$$T' = -\frac{\upsilon_T}{\sigma_k} \nabla k \tag{7}$$

where the turbulent Prandtl number for kinetic energy is generally taken to be $\sigma_k = 1.0$. This equation assumes that there is a flux of k down the gradient of k due to velocity and pressure fluctuations. In summary, the transport equation for turbulent kinetic energy k is

$$\frac{Dk}{Dt} = \nabla \bullet \left(\frac{\upsilon_T}{\sigma_k} \nabla k \right) + P - \varepsilon \tag{8}$$

The three other terms, $-Dk/Dt$, P, and ε, are in closed form given the turbulent-viscosity hypothesis.

Turbulence consists of high levels of fluctuating vorticity. At any instant, vortical motion called eddies are present in the flow. These eddies range in size from the largest geometrical scales of the flow such as tank diameter down to small eddies where molecular diffusion dominates. The eddies are continuously evolving, and the superposition of their induced motions leads to the fluctuating waves. In this situation, turbulent kinetic energy is dissipated from the largest eddies down to the smallest through a process called energy cascade. In order to maintain the turbulence, a constant supply of energy must be fed to the turbulent fluctuations at the largest scales from the mean motions, where it is driven by a jet pump or mechanical agitator. Thus, turbulent energy dissipation rate ε is viewed as the energy-flow rate in the cascade, and it is determined by the large-scale motions, independent of the viscosity at high Reynolds number. Consequently, the transport equation for ε is best considered as being entirely empirical. That is,

$$\frac{D\varepsilon}{Dt} = \nabla \bullet \left(\frac{\upsilon_T}{\sigma_\varepsilon} \nabla \varepsilon \right) + C_1 \left(\frac{\varepsilon}{k} \right) P - C_2 \frac{\varepsilon^2}{k} \tag{9}$$

where the turbulent viscosity is

$$\upsilon_T = C_\mu \frac{k^2}{\varepsilon} \tag{10}$$

where C_μ = 0.09.

It is noted that the turbulent viscosity coefficient C_μ of 0.09 in the two-equation model (Eq. (10)) can be derived under the log-law [Dimenna and Lee, 2011]. From these results, the two-equation turbulence model is good for the bulk model including the log-law shear region, but it will not be good for the flow within the laminar sublayer close to the wall as shown in the previous work [Lee et al., 2008].

Based on the performance criteria discussed earlier, a three-dimensional computational approach was taken to compute flow fields driven by a mechanical agitator. The governing equations as described previously were solved simultaneously by using a commercial CFD code, Fluent™. A prototypic geometry for the agitator and hopper tank was created by a non-orthogonal control volume method in the CFD computational environment.

The analyses were based on the steady-state model for computational efficiency. The main solution methodologies and modeling assumptions were as follows:

- The fluid temperature is isothermally kept at 75 F, neglecting the hydration heat generation of the cementitious material during the agitator stirring process.
- The fluid is assumed to be single-phase flow.
- The fluid behavior is assumed to follow the Bingham plastic model as discussed earlier.
- The present model was based on the 45^o pitched four-blade agitator and tank with no internal solid structures.
- The modeling simulations used three-dimensional steady-state, isothermal governing equations with multiple reference frames (MRF).
- For the steady-state model, the top liquid surface was assumed to be frictionless and flat.

As mentioned above, the steady-state model assumes that free surface remains flat and slip wall. If the agitator rotates in a clockwise direction (as viewed from above), a large axial convection flow moves upward due to the rotation of the pitched blade. When the liquid level becomes low enough to get air pull-through due to vortex formation near the tips of the agitator blades, air will be drawn into the blade zone. An empirical equation (Schrock et al, 1985) is available in the literature to estimate the minimum liquid level which prevents air entrainment into the blade zone of the agitator. They empirically correlated the equation for critical liquid level (H_c) in terms of Froude number (F_r) and fluid properties to get air pull-through from the free surface to the water liquid region. The empirical equation for the critical liquid height is

$$H_c = 0.8513 D_B (F_r)^{0.5} \left(\frac{\rho_f}{\rho_f - \rho_a} \right)^{0.25} \tag{11}$$

where $F_r = \left(\frac{U}{\sqrt{gD_B}} \right)$ (12)

U = Maximum downward fluid velocity at the blade
D_B = blade diameter
ρ_f = liquid density
ρ_a = air density

Tank liquid level above the pitched blade was a significant parameter. As the tank liquid level becomes lower, vortex formation can result in air being drawn into the blade zone of the agitator as shown in Fig. 5. This can cause degradation of stirring capability in the tank since additional momentum is dissipated by the air entrainment near the rotating blade area. Therefore, a minimum liquid level must be estimated to avoid entraining air into the bulk fluid zone. Using the empirical correlation for air entrainment through the vortex formation, equation (11), the liquid level required to avoid air pull-through under the phase-2 agitator was estimated as a function of agitator speed as shown in Table 5. The results show that about a 10 in liquid level above the agitator blades is required to prevent air pull-through from the free surface to the agitator region. It is noted that when about 15 in fluid level above the agitator blade is kept during the hopper tank operation with the rotating speeds of 69 to 200 rpm, air pull-through entrainment through the top fluid surface will not occur.

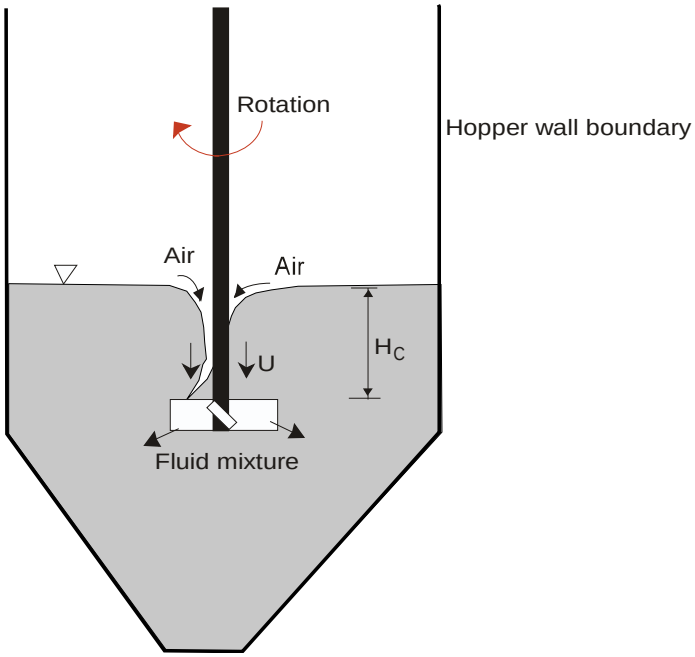

Figure 5. Air entrainment from the top surface of the hopper via vortex formation driven by the pitched blades.

Table 5. Conservative estimation of minimum liquid height to prevent the air pull-through from the top free surface due to the propeller-type phase-2 agitator motion

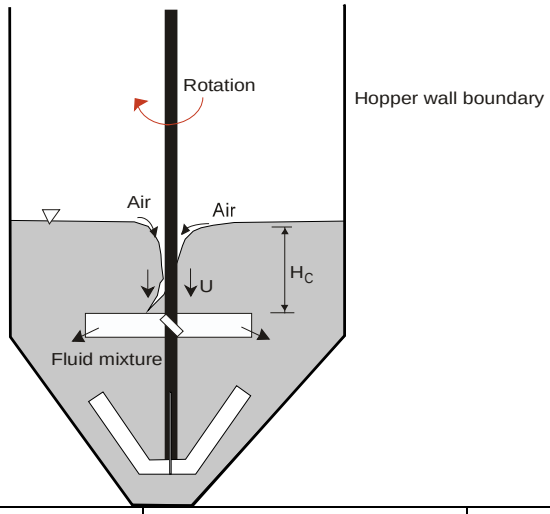

Agitator speed		Froud number (Fr) as defined by Eq. (8)	Min. liquid height above the agitator blade (H_c)* (inches)	Liquid height above the agitator blade for the phase-2 calculations (inches)
(ft/min)	(rpm)			
508	69	0.14	8.0	About 15
1026	140	0.15	8.5	
1466	200	0.17	9.0	

Note: *Based on water-air correlation

In summary, the governing equations to be solved by the CFD approach are one continuity equation, three momentum equations for the three component directions (x, y, and z directions), and in case of turbulent flow regime, two transport equations for the two turbulence quantities, namely κ and ε. As a constitutive relation, the Bingham plastic model was used to estimate the viscous shear stress in the tank domain, assuming that it would give an acceptable representation of the grout material characteristics. The sensitivity studies are performed using typical yield stress for different speeds and different elevations of each agitator.

Three-dimensional steady-state numerical simulations are made for the hopper modeling study by taking two modeling steps. One is the initial phase-1 model for a simple single-stage radial agitator to perform the initial scoping calculations of flow patterns for various operating conditions and different yield stresses. The calculated flow patterns will be provided as design input for the phase-2 agitator. The other is the phase-2 agitator model to evaluate the flow patterns and power consumptions of the two-stage agitator design for different operating conditions.

The computational domain and meshes defined for the modeling analysis are shown in Fig. 6. The number of the established computational meshes for the entire tank domain of the

phase-1 model is about 7.5 x 10^5 nodes. Typical computational meshes established for the phase-2 simulation are shown in Fig. 7. The number of the established computational meshes for the phase-2 model is about 1.0 x 10^6 nodes. This number was established from sensitivity studies of computational meshes. Mesh density is significantly higher in the vicinity of the agitator blades to capture the flow behavior relative to the sharp blade region. The characteristic mesh dimension is much greater in regions far from the agitator and other solid surfaces to keep the total number of nodes manageable.

Range of operating conditions such as different yield stresses, rotational agitator speeds, and agitator elevations were considered to perform the sensitivity calculations for the flow patterns with respect to the baseline modeling conditions. The modeling cases used for the present steady-state analysis are summarized in Table 6.

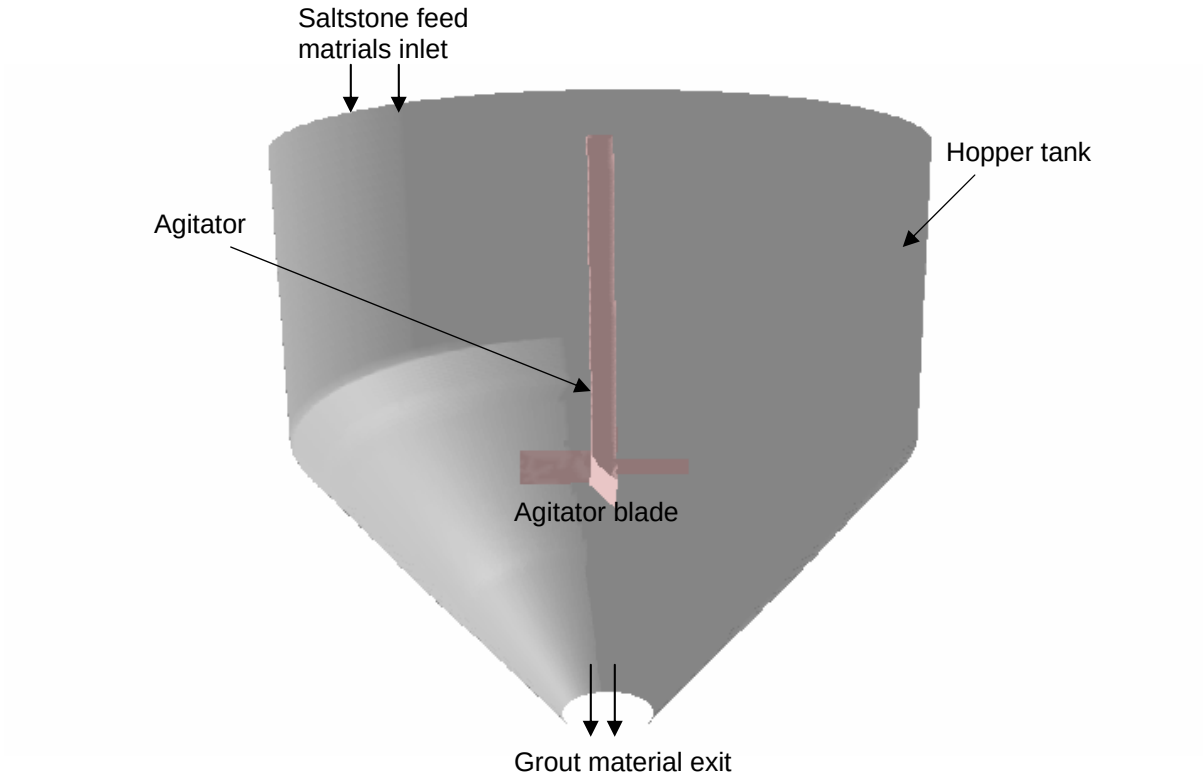

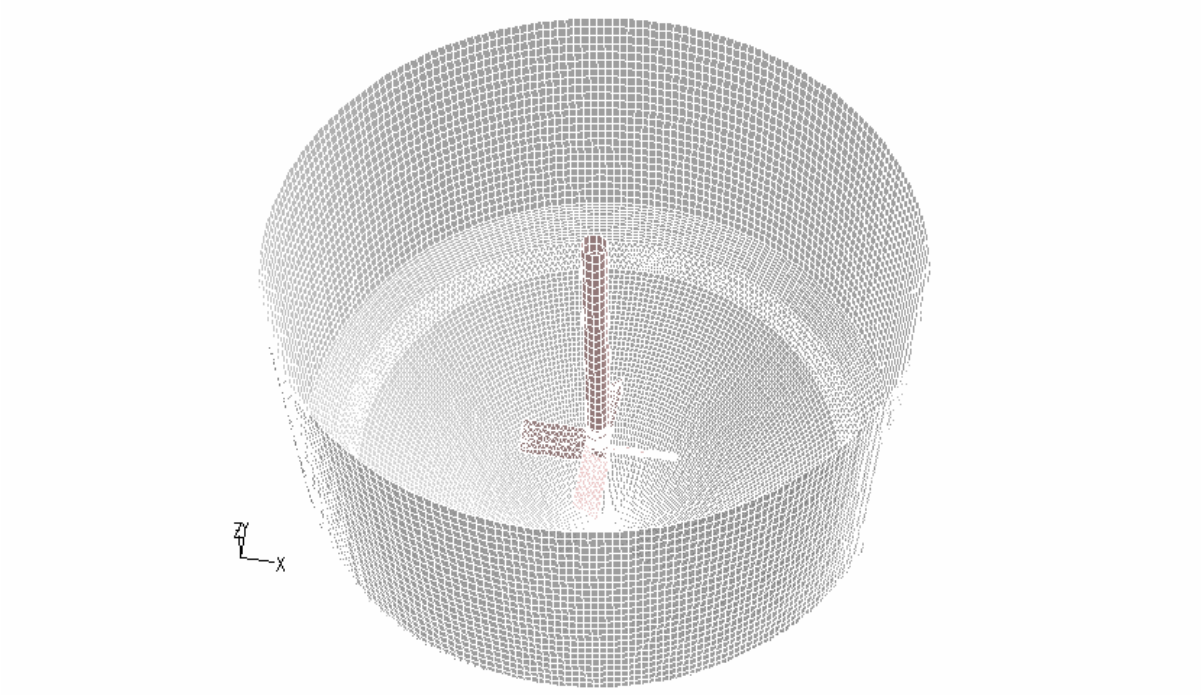

Figure 6. Computational domain and meshes used for the baseline modeling calculations (0.75 million meshes)

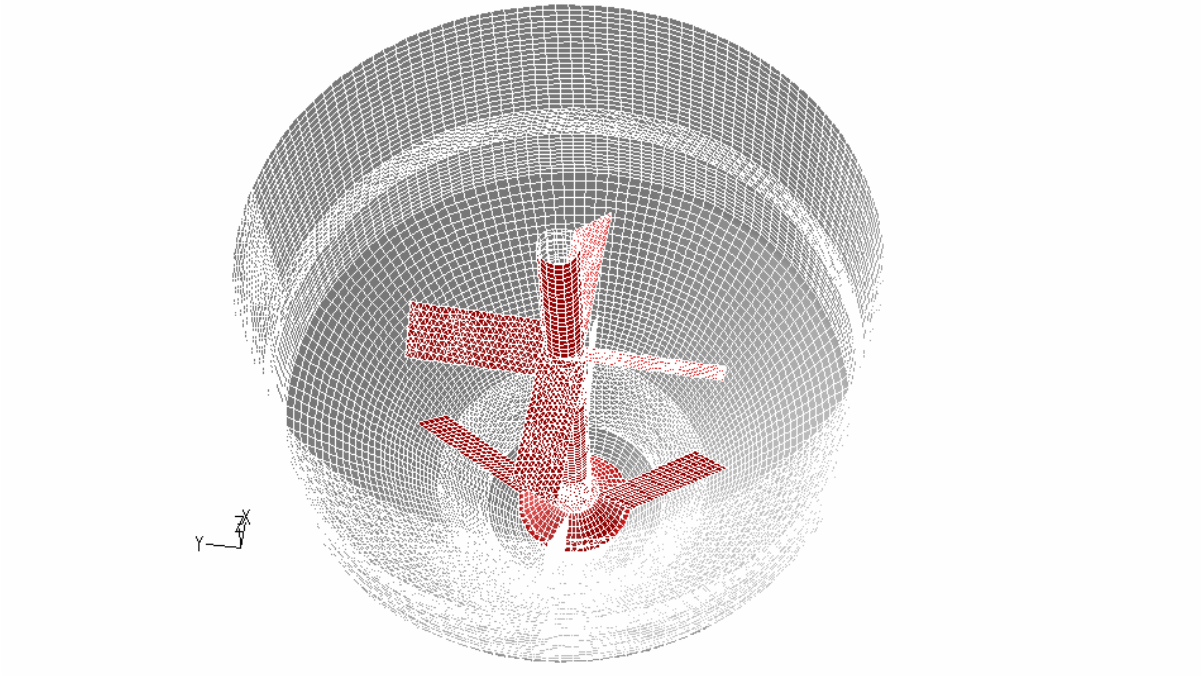

Figure 7. Computational volume meshes used for the phase-2 modeling calculations (1.0 million meshes)

Table 6. Modeling cases considered for the analysis

Model	Cases	Rotational speed (rpm), [Yield stress, Pa]	Agitator elevation from the tank bottom (inches)	Purposes
Phase-1 model (Single-stage propeller blade as shown in Fig. 2)	Case A1 (Baseline)	175 [21]	22	To perform the initial scoping calculation for basic flow patterns and characteristics associated with agitator performance requirements
	Case A2	246 [0.01, 1, 10, 21]	22	To perform the sensitivity analyses of flow patterns for a range of yield stresses and agitator speeds
Phase-2 model (Two-stage propeller blade as shown in Fig. 3)	Case B1 (Baseline)	69.3 [1, 5, 10, 21]	10, 6	To conduct the baseline performance analysis for basic flow patterns / shear rate profiles and to perform the sensitivity analysis for a range of yield stresses
	Case B2	69.3, 140, 200 [1, 5, 10, 21]	10, 6	To perform the sensitivity analysis for agitator speed, elevation, and a range of yield stresses

4.0 RESULTS AND DISCUSSIONS

The Saltstone hopper models have been developed by a CFD approach to evaluate the flow pattern behavior with a mechanical agitator and to estimate the flow residence time in the grout hopper tank. For the CFD modeling calculations, different agitator designs and configurations were considered for examining the impact of fluid stirring performance for the initial baseline configurations. As the performance criteria, shear rate profile and flow pattern were used as a key indicator of the grout material movement from the rotating agitator region into the remote wall boundary zone in the fluid domain of the hopper tank. If the shear rate for the grout materials gets smaller than 10^{-5} (1/sec), the materials will not be mixed adequately and may be solidified during the process period. Estimation of flow patterns was used as the degree of stirring efficiency from the grout material interaction with blade passage and from the residence time of the tank contents to prevent vortex-type pull-through. The flow pattern was estimated from the flow path lines of the feed materials obtained by Lagrangian integration along the fluid movement starting from the material feed inlet. Benchmarking analysis of the modeling predictions against the test results is not included in this task scope.

As mentioned previously, the work used two modeling steps for the modeling calculations. One step is to develop a simple single-stage agitator tank model to evaluate the initial scoping calculations and to provide design guideline for next phase agitator. It consists of 45^o pitched, four flat-plate blades. And each blade has 14 in diameter. The other is to develop the phase-2 agitator model to conduct the stirring performance and sensitivity analyses, including the estimate of power consumptions. The modeling domain to be used for the present analysis is presented in Figs. 6 and 7. Nominal design and operating conditions for the pahse-1 and phase-2 agitators used for the hopper tank modeling and analysis are presented in Table 1 and Table 2. Based on the modeling domain and operating conditions, flow pattern calculations driven by the agitators were performed. When 150 gpm material flows into the hopper tank through the 10-in pipe at top left corner and exits via the 8-in tank bottom, the computational models were run in steady state mode for a rotating agitator to allow the stirred flow profile to develop steady-state flow pattern. Table 6 shows all cases considered for the present modeling analysis.

4.1 PHASE-1 MODELING RESULTS

As discussed earlier, Case A1 was selected as the baseline agitator configuration, since a single propeller-type agitator is available for the initial calculations in stirring up the grout materials. Figure 8 shows qualitative flow patterns driven by the propeller blades as observed by numerical simulations for 5 Pa yield stress and 175 rpm agitator speed. When there is no grout feed flow at the top left corner of the hopper, symmetrical flow patterns with respect to the rotating agitator are developed from the hopper center to the wall boundary as expected. The results show that the rotating agitator submerged in a stationary hopper generates two primary flow motions consisting of axial convective flow from the 45^o pitched flat surface and vortex flow at the tip of blade. The modeling results are consistent with the literature results [Tatterson, 1991]. Case A2 has the same agitator as Case A1does, but it uses different yield stresses and speeds for the assessment of the parametric impact on the flow patterns. Figure 9 compares velocity distributions for grout materials with two different yield stresses under 175 rpm agitator speed at the central plane of the hopper. The results clearly show that when the material yield stress increases from 1 Pa to 10 Pa, much of the fluid in the tank was unaffected by the blade passage and the vortex system generated by the phase-1 propeller blade was not shed by the blade. The blade diameter for the phase-1 agitator is 14 inches.

When the phase-1 single-stage agitator mixes 1 Pa yield stress materials with 175 rpm speed inside the hopper tank, flow patterns and stream path lines are presented in Fig. 10. The pathlines were obtained by Lagrangian integration along the flow motion. When the material yield stress increases from 1 Pa to a maximum value of 21 Pa, flow patterns are significantly changed in terms of local velocity and flow pathlines as shown in Figs. 11 and 12. It is indicated that when the yield stress becomes higher, the fluid become less affected by the agitator passage due to the higher shear stress as shown in Eq. (6). The shear rate profiles for various yield stresses are compared in a quantitative way in Fig. 13 when the phase-1 agitator mixes the hopper materials. The results show that the initial phase-1 single-stage agitator does not provide adequate stirring performance in terms of flow performance criteria since shear rates decreases rapidly for yield stresses larger than 10 Pa and they are well below 10^{-5} (1/sec) for the remote zone outside the 14-in agitator domain as shown in Fig. 13. The results for shear stresses are quantitatively compared for a range of yield stresses (from 1 Pa to 21 Pa) in Fig. 14. As shown in the figure, the modeling results clearly indicate that the tip of each agitator blade has the highest shear stress since its shear rate is the highest as presented in Fig. 13. The shear stress at the blade wall is

closely related to the erosion characteristics of agitator blades and tank wall. These results are consistent with the literature information [Lee et al., 2003, Tatterson, 1991].

Sensitivity analysis for different agitator speeds was performed for the assessment of the fluid movement generated by the phase-1 single-stage agitator. Shear rate profiles for the two different agitator speeds under maximum yield stress (21 Pa) are compared along the horizontal line A-A' crossing the agitator blade in Fig. 15. As shown in the figure, fluid movement for the remote region was not affected by the increase of the agitator speed for high yield stress. However, when fluid yield stress becomes smaller, shear rates are affected significantly, especially, near the wall boundary region as indicated in Fig. 16.

The baseline modeling study was based on the open tank system, which feeds the materials into the tank from the top left corner and discharges via the tank bottom at the same rate as the inlet. In this case, when the material feed inlet location changes from the top corner to the top center of the hopper under the phase-1 baseline modeling conditions, the impact of the material inlet location on the flow patterns was evaluated under the Bingham plastic non-Newtonian models with two different yield stresses. Figure 17 compares shear rates for two different flow inlet locations along the horizontal line A-A' crossing the agitator blade. The results show that shear rates were clearly increased by changing the location of material feed inlet from the corner to the center of the tank, but high yield stress fluid is still stagnant near the wall boundary due to the small size of the agitator blade. All the phase-1 results indicate that when yield stress of the Saltstone feed materials is higher than 10 Pa, the size of the agitator blade has to be increased for the enhancement of the shear rates near the hopper wall to prevent the solidification of the grout materials during the stirring operation. In this case, the power consumption P for keeping the feed materials of flowrate Q in motion is directly related to the blade size D_B. When the agitator speed is N revolutions per unit time, the power P becomes

$$P = 0.5 Q \rho_f (\pi N D_B)^2 \quad (13)$$

The results for the phase-1 baseline modeling calculations are summarized as follows:

- The modeling results clearly show that when the tank fluid has a higher viscosity, more fluid in the tank was unaffected by the blade passage and that the vortex system was not shed efficiently by the agitator blade.
- It is noted that the mass, which flowed inside the rotating agitator zone, remained with the blade considerably longer than the fluid passing through the clearance area because of the high wall shear as shown in Fig. 13. These results are consistent with the literature information [Tatterson, 1991]
- The flow patterns for the viscous fluid with high yield stress indicated very little disturbance of the fluid in the wall boundary or the clearance area near the wall.

Based on the initial phase-1 results, key parameters for the next phase agitator design are listed for keeping the hopper contents in motion prior to their transfer to the Saltstone processing facility. They are as follows:

- Blade size needs to be longer and wider to increase the impact of the agitator passage on fluid disturbance toward the wall boundary region remote from the agitator. The size of the agitator should be optimized by its power requirement as defined by Eq. (13).
- Flow entrance location moves to the center of the hopper tank to maximize its direct interactions with the agitator during the fluid residence time in the tank.

- When the cementitious fluid has a high yield stress, a two-stage agitator consisting of radial blades and propeller blades is required to keep tank fluid in motion and longer fluid residence time.

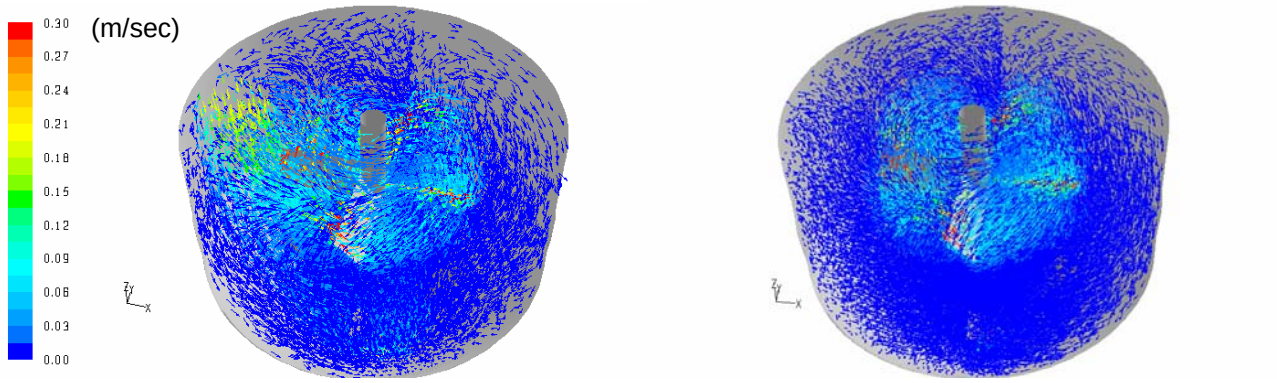

(150 gpm feed inlet flow) (no feed inlet flow)

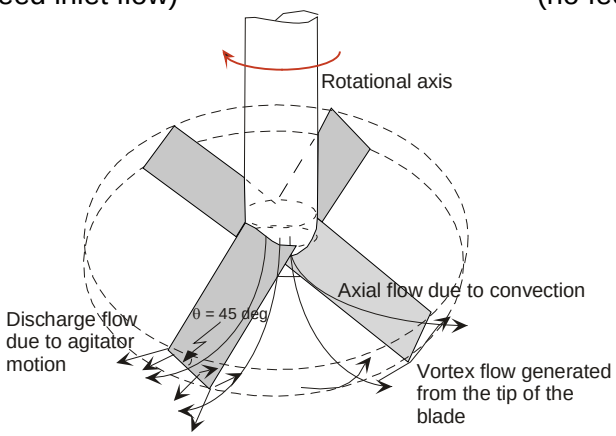

Figure 8. Qualitative flow patterns driven by the propeller blades as observed by numerical simulations for 5 Pa yield stress and 69 rpm agitator speed

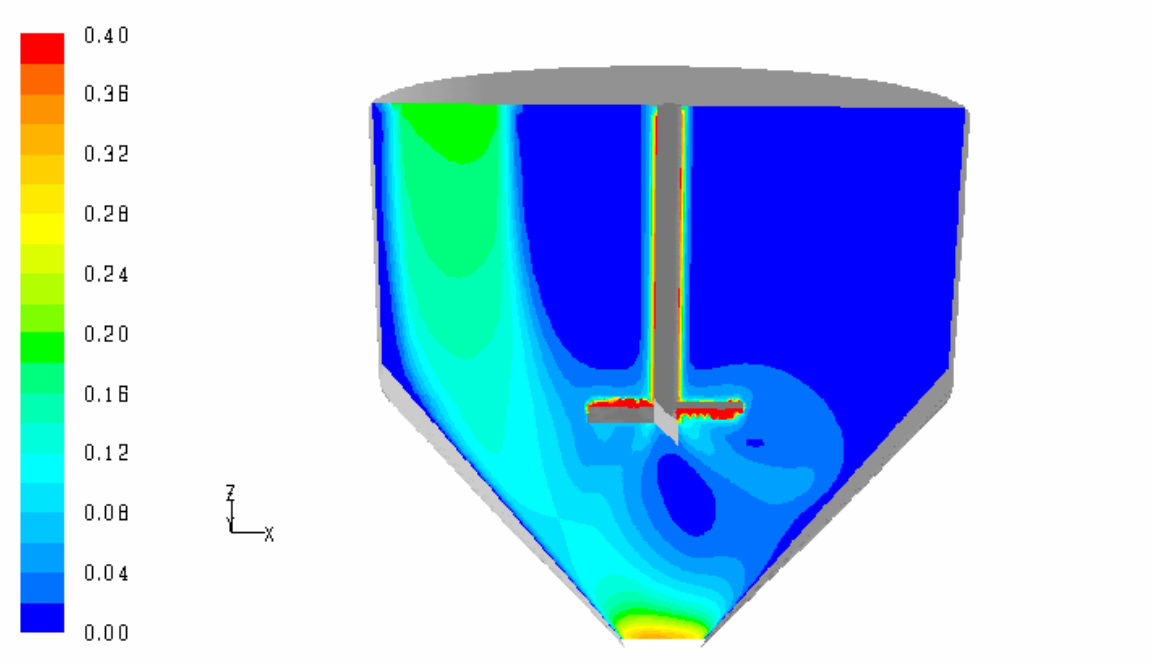

(Yield stress = 1 Pa)

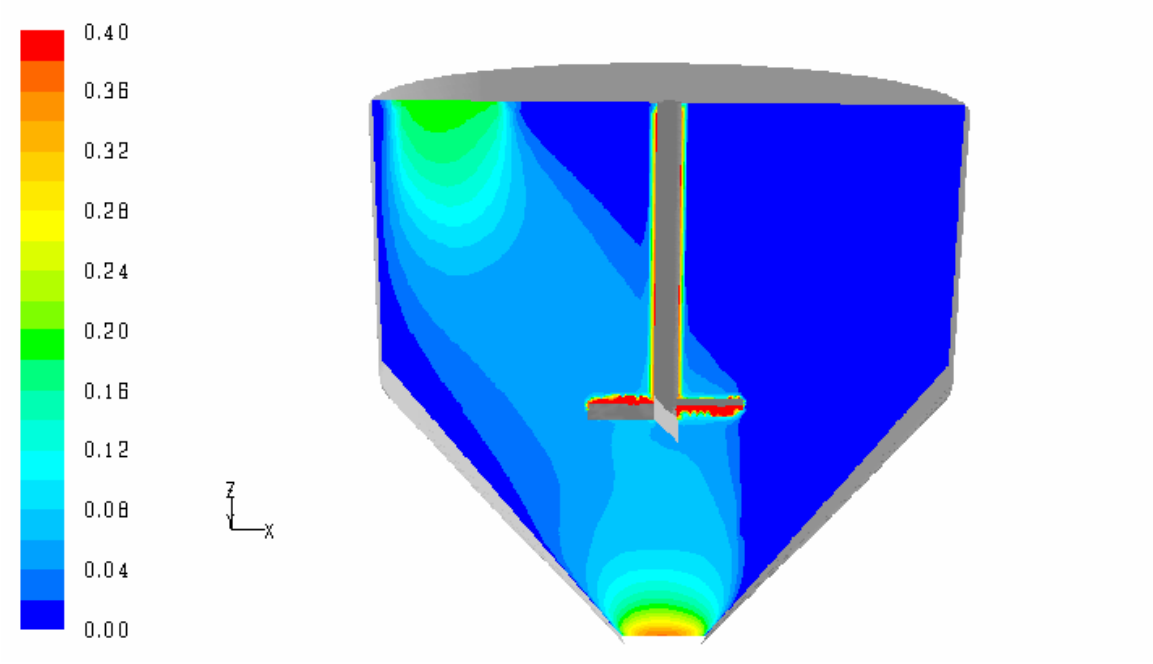

(Yield stress = 10 Pa)

Figure 9. Comparison of velocity distributions at the mid plane of the hopper for grout materials with two different yield stresses under 175 rpm agitator speed with 150 gpm feed flow.

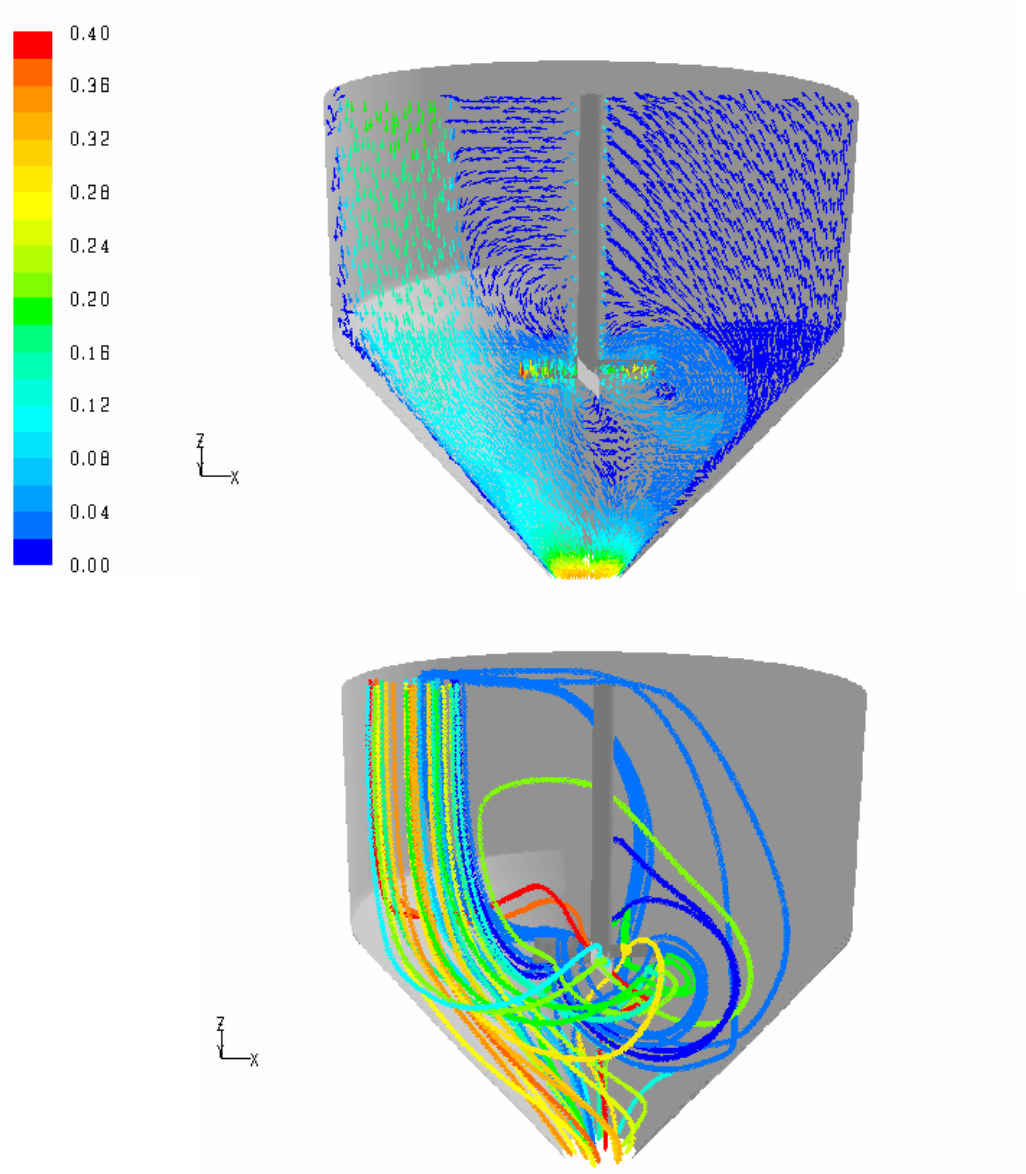

Figure 10. Flow patterns and stream path lines for 1 Pa yield stress grout material inside the hopper tank with 175 rpm agitator speed.

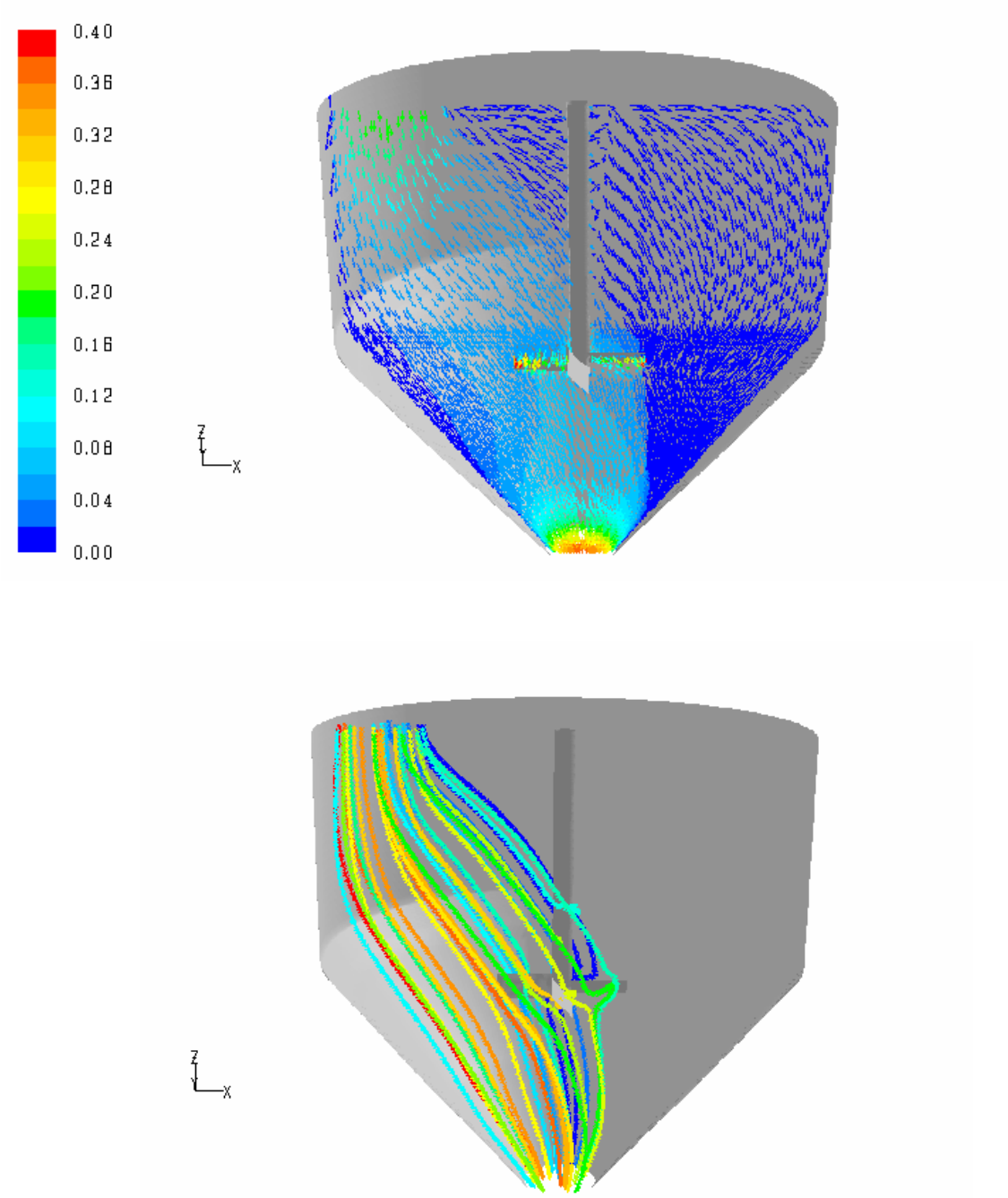

Figure 11. Flow patterns and stream path lines for 10 Pa yield stress grout material inside the hopper tank with 175 rpm agitator speed.

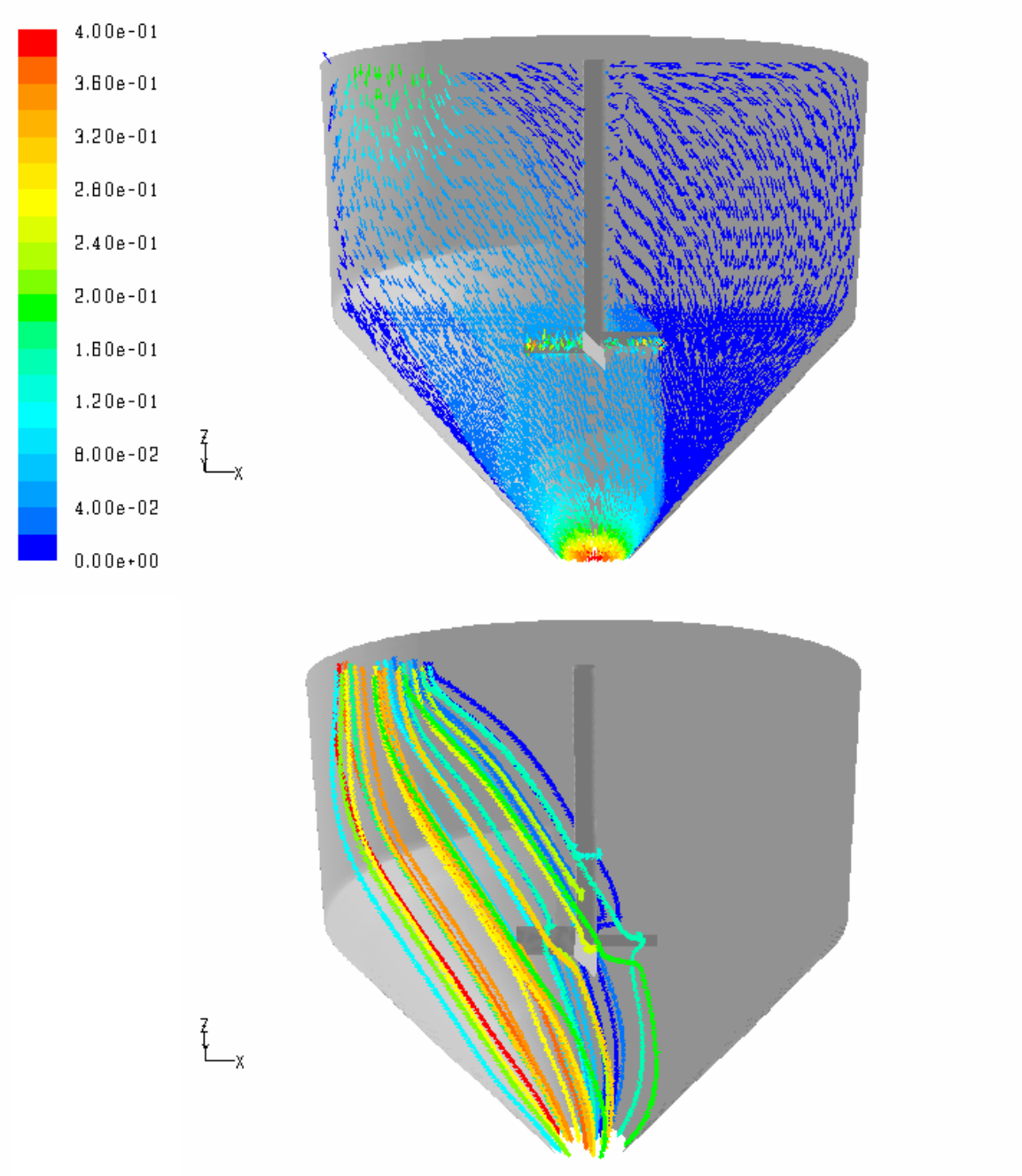

Figure 12. Flow patterns and stream path lines for 21 Pa yield stress grout material inside the hopper tank with 175 rpm agitator speed.

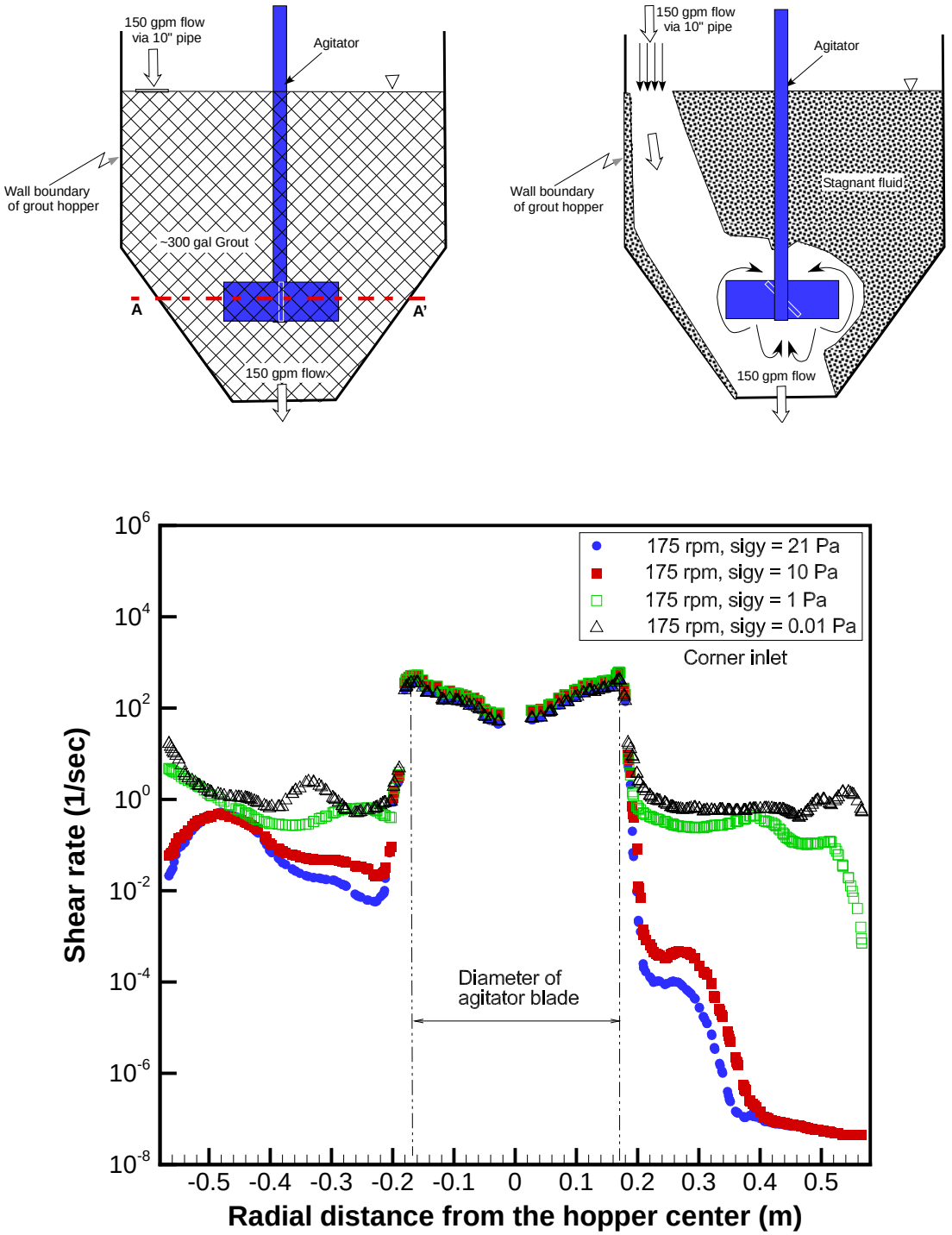

Figure 13. Quantitative comparison of shear rates along the line A-A' for various grout yield stresses under the phase-1 single-stage agitator with 175 rpm.

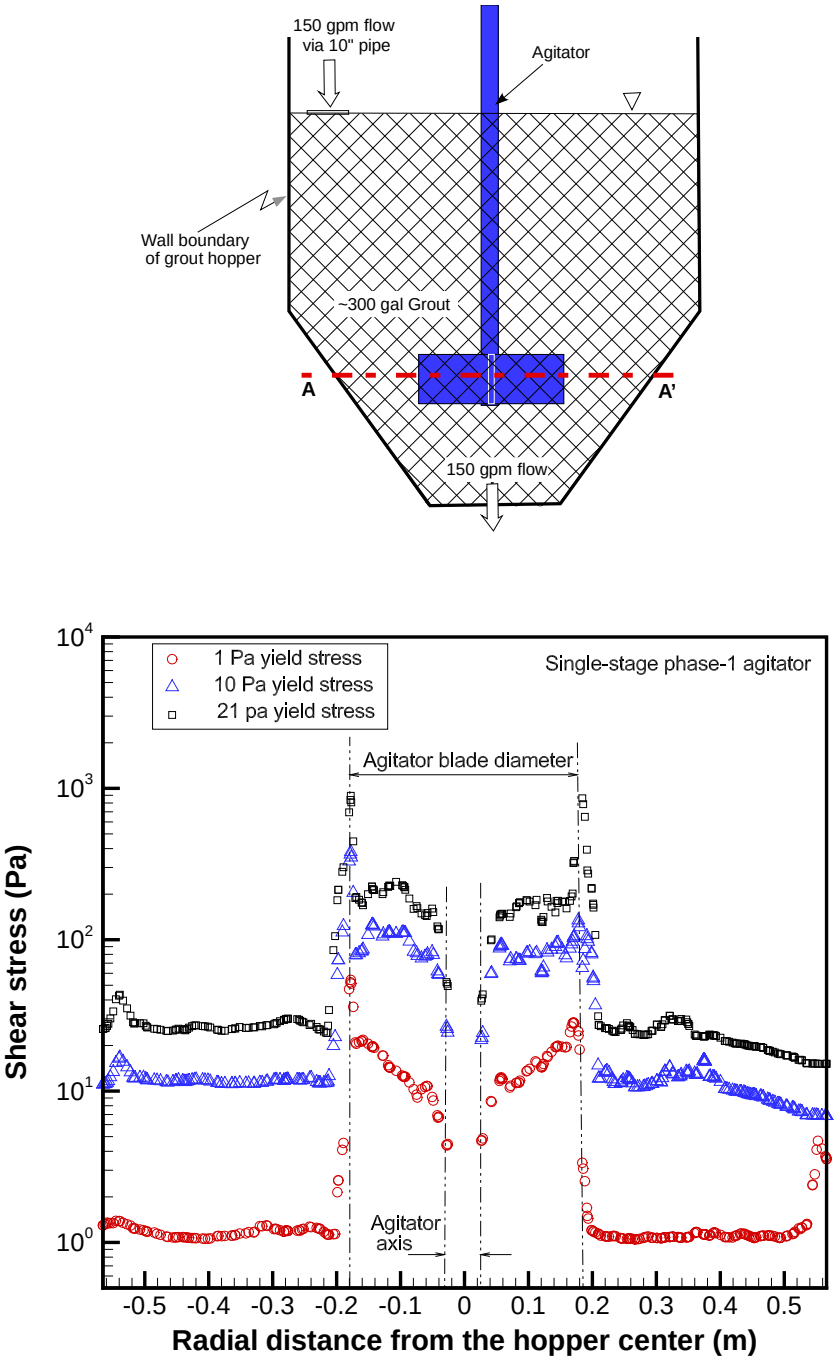

Figure 14. Comparison of shear stresses along the line A-A' for various yield stresses inside the hopper tank with 175 rpm agitator speed with 150 gpm feed flow.

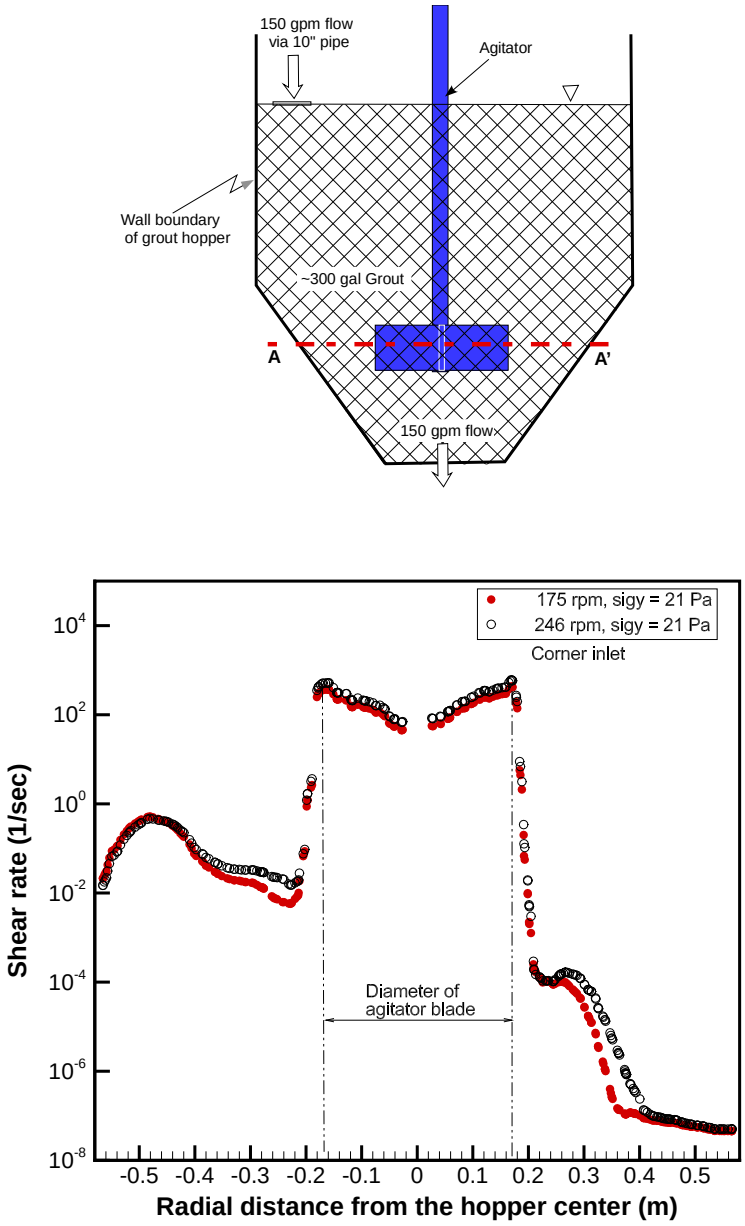

Figure 15. Comparison of shear rates for the two different agitator speeds under the high yield stress (21 Pa) with 150 gpm feed flow along the horizontal line A-A' crossing the agitator blade

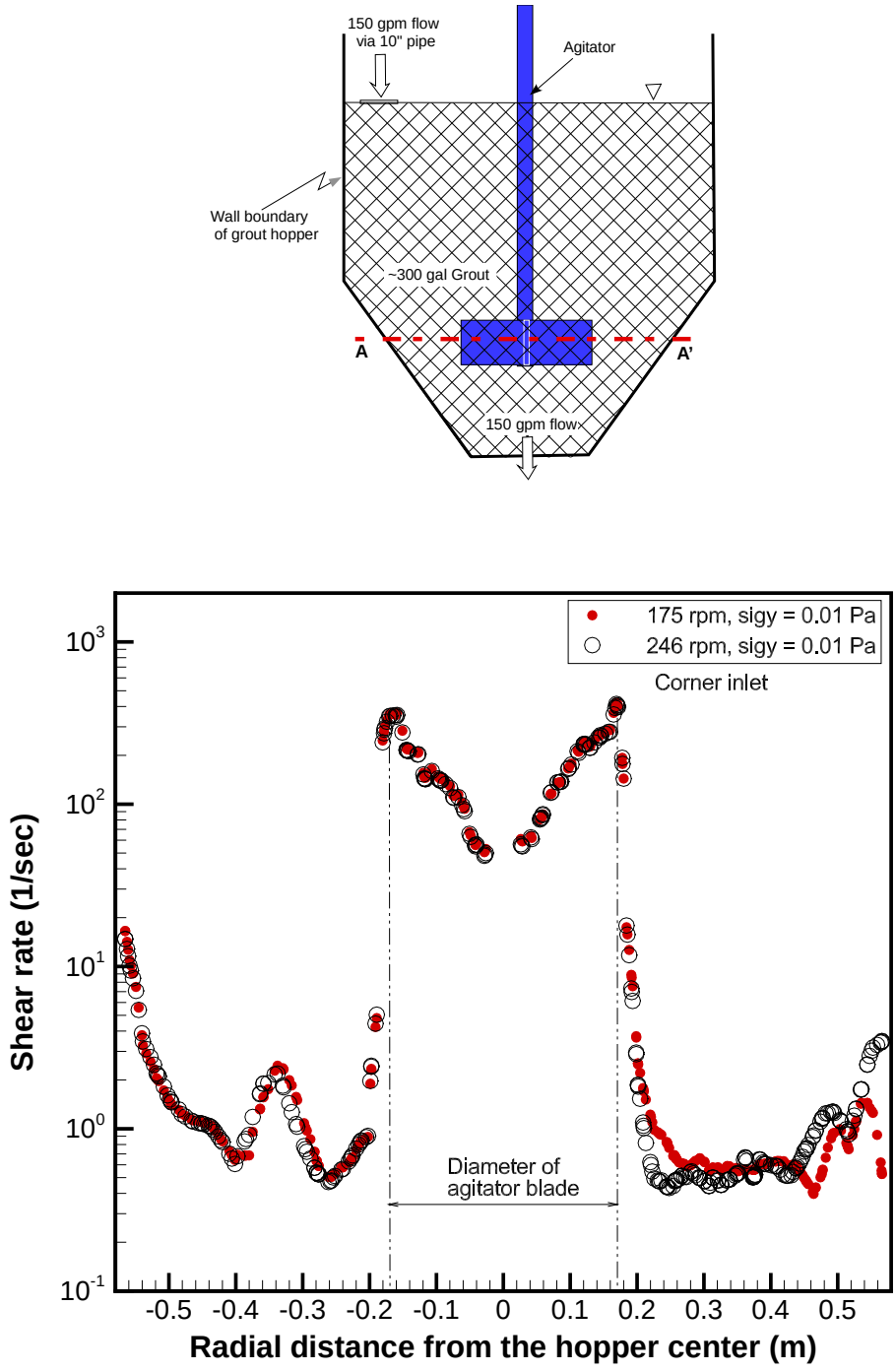

Figure 16. Comparison of shear rates for the two different agitator speeds under the low yield stress (0.01 Pa) along the horizontal line A-A' crossing the agitator blade

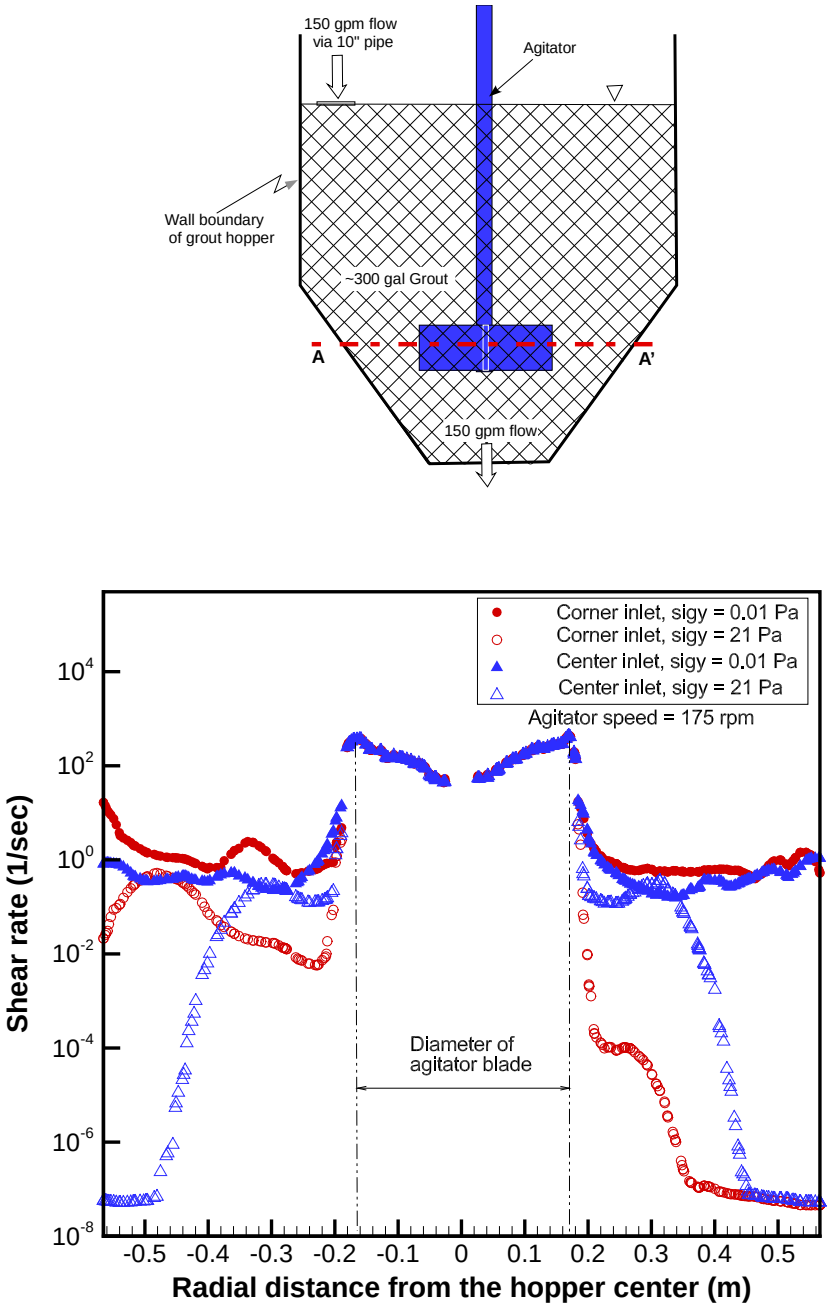

Figure 17. Comparison of shear rates for two different flow inlet locations along the horizontal line A-A' crossing the agitator blade under the Bingham plastic non-Newtonian models with two different yield stresses

4.2 PHASE-2 MODELING RESULTS

Based on the initial phase-1 results, a two-stage agitator with longer and wider blades is selected for the phase-2 performance analysis. It consists of the upper and lower agitator blades as shown in Fig. 3. As shown in the figure, the upper one has four 45^{o} pitched propeller blades, and the lower has four vertical flat-plate radial blades. For the performance analysis, the flow patterns and shear rate profiles were primarily used as the flow acceptance criteria to allow adequate stirring prior to transfer of the hopper contents. The criteria will minimize stagnation zones inside the hopper so that the feed materials are mixed and prevented from being solidified in a reasonable way during the stirring process.

As shown in Table 2, the performance calculations for two different heights of agitator, 10 and 6 in above tank bottom, were conducted to examine the impact of agitator elevation on the stirring performance for given agitator configurations, keeping the 27 in distance between impellers fixed as shown in Fig. 3. The phase-2 agitator located 10 in above the tank bottom exit will be used as the phase-2 baseline modeling case, Case B1. For a given agitator elevation, three different agitator speeds, 140 and 200 rpm, and the reference speed of 69.3 rpm, were considered for the assessment of the speed impact on the tank stirring performance for a range of fluid yield stresses in terms of flow patterns and shear rates. Shear rates and viscous stresses for the modeling domain were calculated from the simultaneous solutions of the flow governing equations combined with Bingham plastic equation as a constitutive relation for viscosity. The results will be provided for the operation and design guidelines of the hopper tank system. All modeling cases considered for the phase-2 study are provided in Table 6.

For the agitator speed of 69.3 rpm and the agitator elevation of 10 inches above the tank bottom, the baseline calculations for the phase-2 agitator were performed for a range of yield stresses (from 1 to 21 Pa), which corresponds to Case B1 in Table 6. For the phase-2 performance analysis, 5 Pa yield stress was used as the baseline and nominal yield stress. Figure 18 compares the primary flow path lines starting from the 150 gpm inlet flowrate for various yield stresses at 69.3 rpm agitator speed. The corresponding velocity distributions are compared in Fig. 19. When the material yield stress changes from 21 Pa to 1 Pa, shear rate profiles are quantitatively compared along the radial direction crossing the upper agitator in Fig. 20. The results clearly show that as the yield stress becomes smaller than 5 Pa, shear rate for 69 rpm rotational speed increased rapidly near the tank wall region so that the agitator keeps fluid in motion more efficiently toward the remote region.

Sensitivity analysis for the agitator speed was performed to investigate the impact on the flow patterns for the same baseline operating conditions of case B1 other than the speed. The results show that when the agitator speed increases from the baseline value of 69.3 rpm to 140 rpm, the fluid is kept in motion more actively in terms of the Lagrangian fluid path lines, compared to those of the baseline speed. Although the flow regime for the phase-2 modeling conditions was found to be turbulent in terms of agitator speed as shown in Table 4, the impact of the turbulent eddy formation on the flow patterns was evaluated. If the flow regime changes from turbulent to laminar, the fluid motion of the tank contents is affected by the agitator rotation with a smaller region. The sensitivity results due to the changes of the agitator speed and the flow regime are presented in Fig. 21. Figure 22 quantitatively compares the impact of the agitator speed on the fluid disturbance at the location of the upper propeller blade, which is 38.8 inches above the tank bottom. When the hopper contents has the baseline yield stress of 5 Pa, comparison of shear rate profiles for different agitator speeds are compared at the locations of the upper and lower blades in Fig. 23. As

shown in these figures, the shear rates at the remote region of the hopper tank are increased by several order of magnitudes with the agitator speed increased from 69.3 rpm to 140 rpm. It is clearly shown that the increase of the agitator speed helps keep the tank contents circulated in larger fluid region.

When agitator elevation is changed from the baseline value of 10 inches above the bank bottom (Case B1) to the minimum level of 6 inches (Case B2) for various yield stresses, primary flow path lines starting from the material feed inlet under the phase-2 agitator speed of 69.3 rpm are qualitatively compared in Fig. 24. For a given yield stress of 5 Pa, comparison of flow shear rates for different agitator speeds is made at two different locations for 6 in elevation of the phase-2 agitator in Fig. 25. Figure 26 compares velocity distributions between two different elevations of the phase-2 agitator at the middle plane of the hopper tank. Primary flow path lines corresponding to the velocity distributions shown in Fig. 26 are compared between two different elevations of the phase-2 agitator for 69.3 rpm agitator speed in Fig. 27. When the agitator speed increases from the baseline speed of 69.3 rpm to 140 rpm for a given yield stress of 5 Pa, comparison of primary flow path lines and residence times of the feed materials with 5 Pa yield stress between two different elevations of the phase-2 agitator is shown in Fig. 28. It is noted that both the fluid residence times for both cases are about the same, about 75 seconds. Figure 29 compares the shear rate profiles of the feed materials with 5 Pa yield stress between two different elevations of the phase-2 agitator at the 39-in vertical location under two different agitator speeds. The modeling results show that the performance indicators, the flow pattern and material residence time, are not sensitive to the elevation of the agitator inside the hopper.

As discussed previously, the shear stress was computed by the Bingham plastic approximation for a given yield stress and plastic consistency, Eq. (6). Figure 30 shows the comparison of shear rate profiles along the radial distance of 38.8 in elevation for various yield stresses under 140 rpm agitator speed. The results show that shear rate for the baseline yield stress of 5 Pa reaches about 0.6 (1/sec) at the wall boundary. The Saltstone material may not be fed into the hopper tank in a continuous way through the top left corner of the tank as modeling here. Figure 31 compares the shear rates along the radial distance of 38.8 in elevation for the nominal flow of 150 gpm flow and no flow through the feed inlet under 140 rpm agitator speed with 5 Pa yield stress materials. It is noted that when there is no feed flow into the hopper, the shear rate profile become symmetrical with respect to the agitator as expected.

When 150 gpm material flow of 5 Pa yield stress is continuously fed into the top left corner of the hopper via 10 in pipe, shear stress and pressure distributions around the agitator are presented in Fig. 32. The calculation results show that the highest shear stress is at the tip of the blades as expected. The modeling results clearly indicate that the lager agitator size and the faster rotational speed are recommended for the increased propagation of agitated flow disturbance to the wall boundary, which increases the fluid residence time to prevent the feed fluid from being discharged without any stirring and increases the shear rates to avoid solidification of stagnant grout prior to transfer of the tank contents.

Power consumptions required to drive the agitator rapidly increases with the agitator size and speed increases. The power consumptions were computed from the shear and pressure forces for different agitator speeds. The computed power was nondimensionalized by the reference power calculated by the agitator speed and size as given by Eq. (13). The power consumptions and the nondimensional power numbers were evaluated as a function of agitator speed for the baseline phase-2 agitator. The results are shown in Fig. 33. The

results indicate that the phase-2 two-stage agitator needs 140 rpm speed for optimum operation, and the motor to drive the agitator requires about 3 HP power.

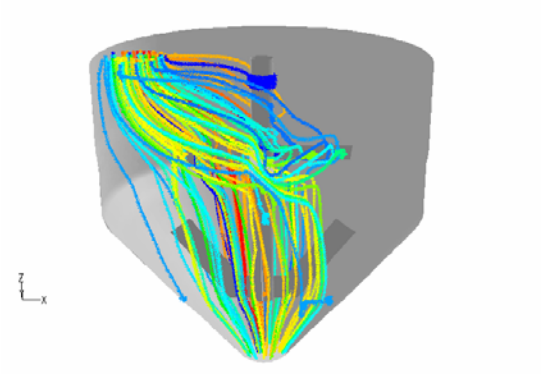

(Yield stress = 21 Pa at 10” elevation)

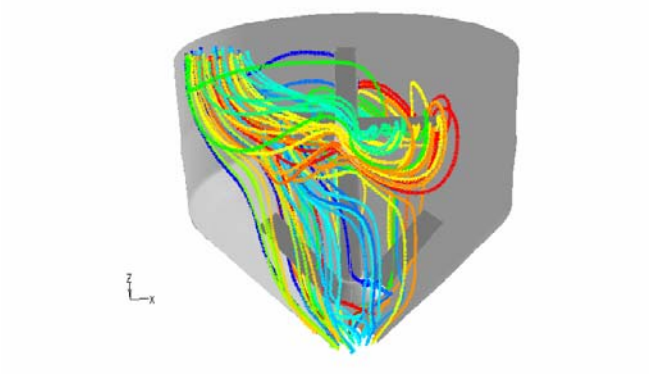

(Yield stress = 5 Pa at 10” elevation)

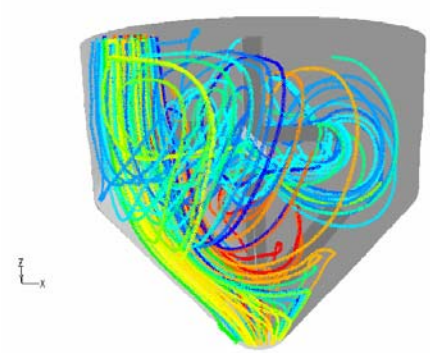

(Yield stress = 1 Pa at 10” elevation)

Figure 18. Primary flow path lines starting from the material feed inlet under the phase-2 agitator speed of 69.3 rpm

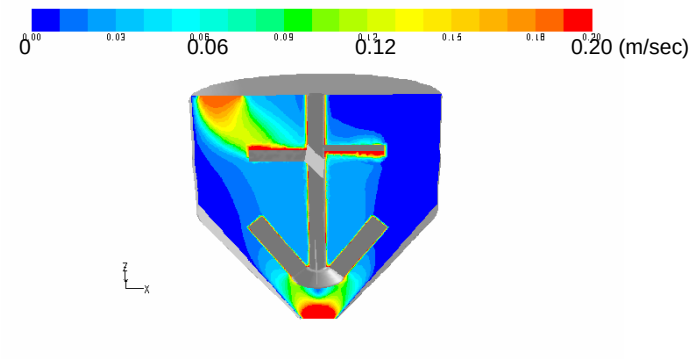

(Yield stress = 21 Pa at 10” elevation)

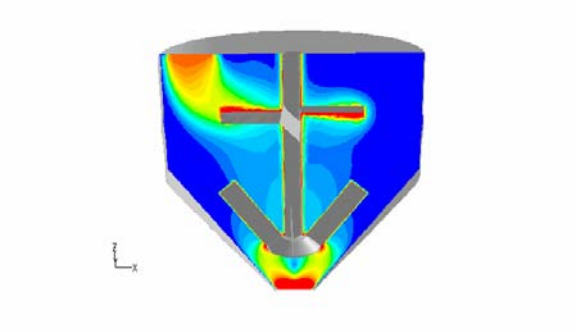

(Yield stress = 5 Pa at 10” elevation)

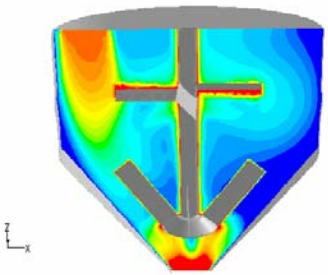

(Yield stress = 1 Pa at 10” elevation)

Figure 19. Velocity distributions for 150 gpm feed flowrate of the grout material through 10 in inlet pipe at top left corner under the phase-2 agitator speed of 69.3 rpm

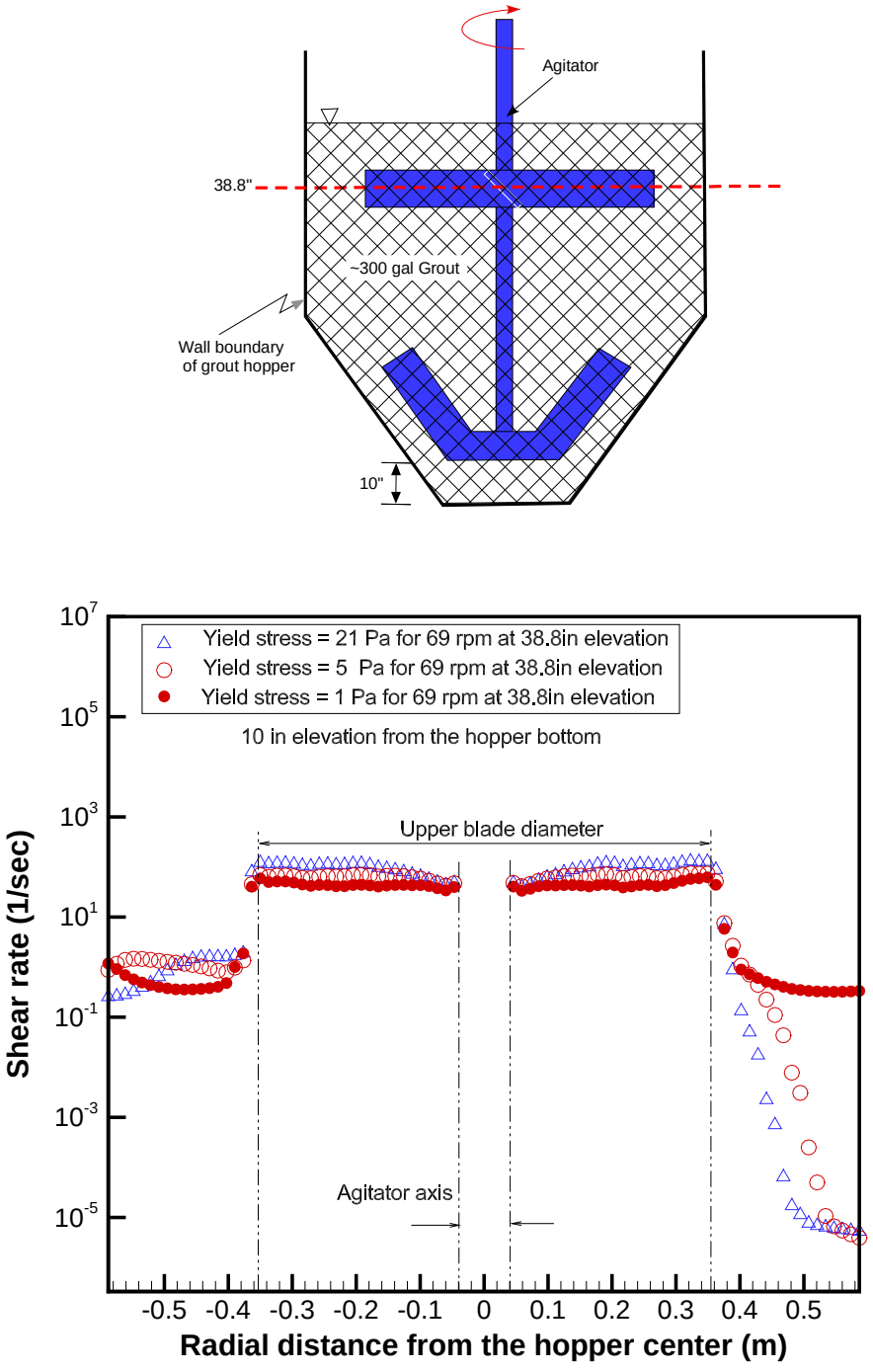

Figure 20. Comparison of shear rates for various yield stresses of Saltstone feed materials under the phase-2 agitator speed of 69.3 rpm located at 10 in above the tank bottom

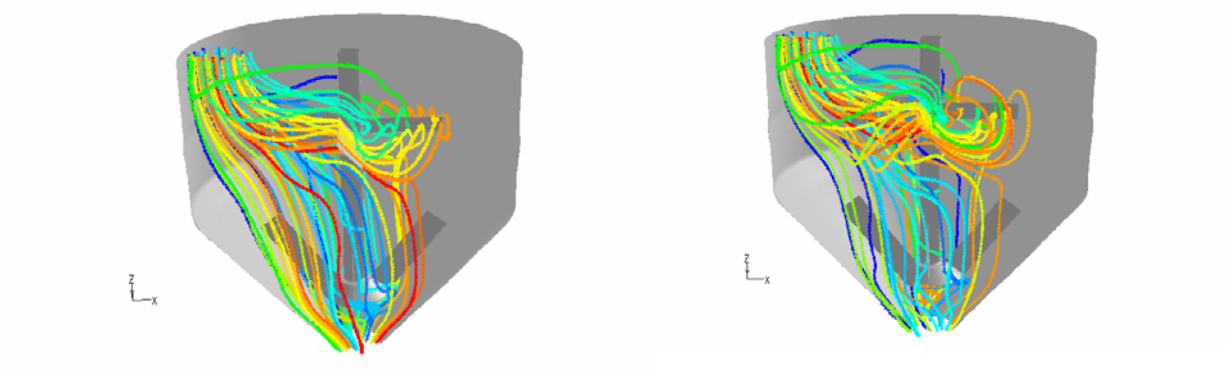

(69 rpm, laminar flow)

(140 rpm, laminar flow)

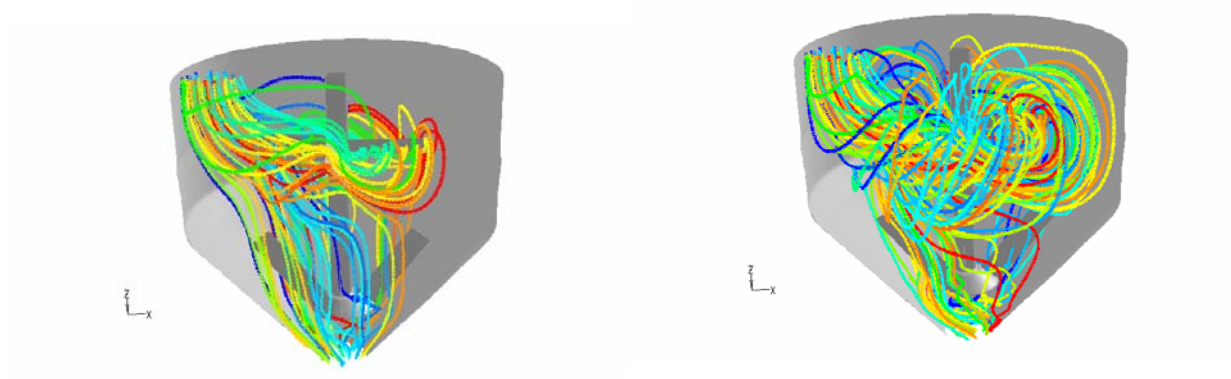

(69 rpm, turbulent flow)

(140 rpm, turbulent flow)

Figure 21. Comparison of flow path lines of feed materials driven by the phase-2 agitator for different speeds and different flow regimes (10” agitator elevation, 5 Pa yield stress).

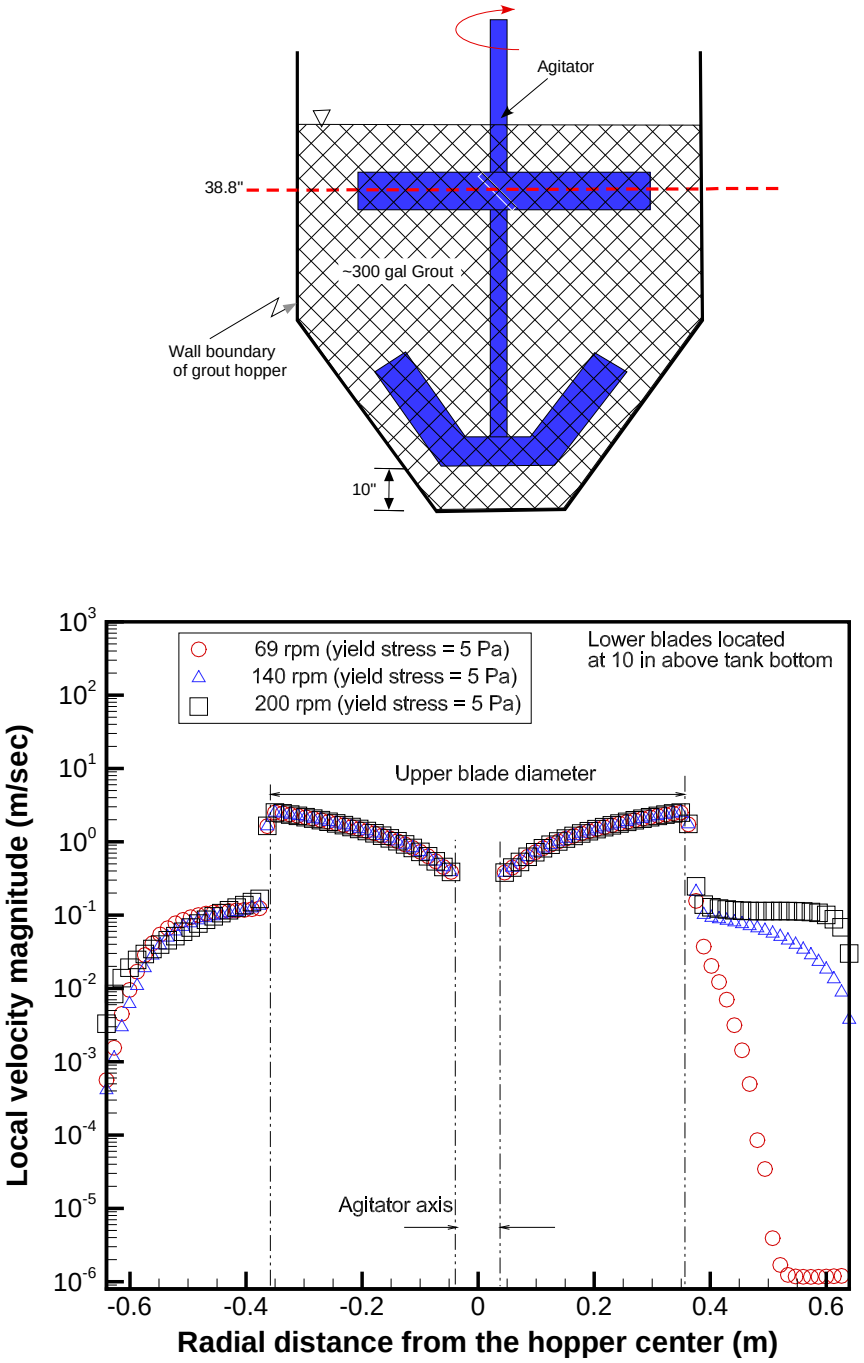

Figure 22. Comparison of local velocity magnitudes driven by phase-2 agitator for different speeds under turbulent flow regime at the location of the upper blade 38.8 in (10 in agitator elevation, 5 Pa yield stress).

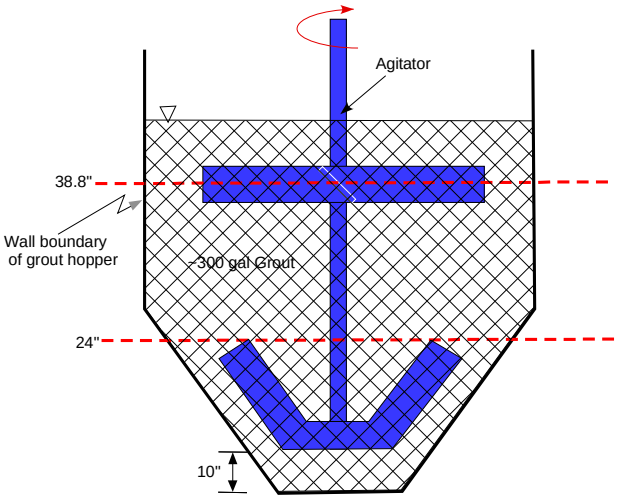

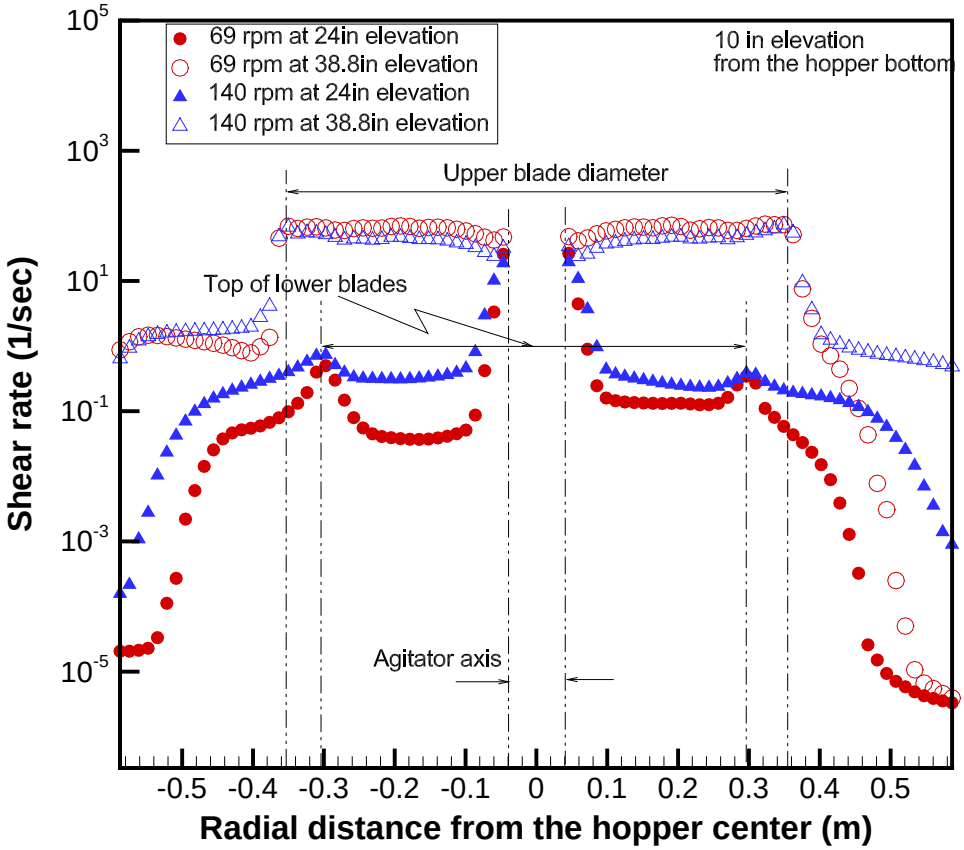

Figure 23. Comparison of turbulent grout flow shear rates for different agitator speeds at different elevations under 5 Pa yield stress

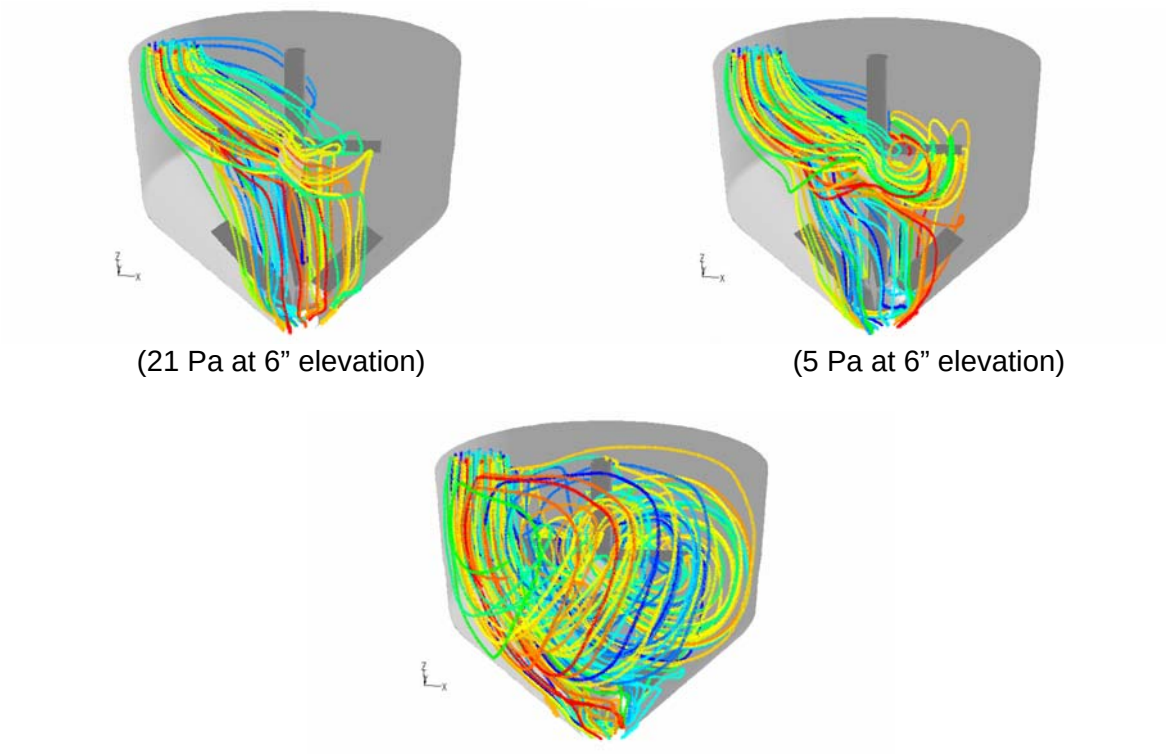

(21 Pa at 6” elevation)

(5 Pa at 6” elevation)

(1 Pa at 6” elevation)

Figure 24. Primary flow path lines starting from the material feed inlet under the phase-2 agitator speed of 69.3 rpm

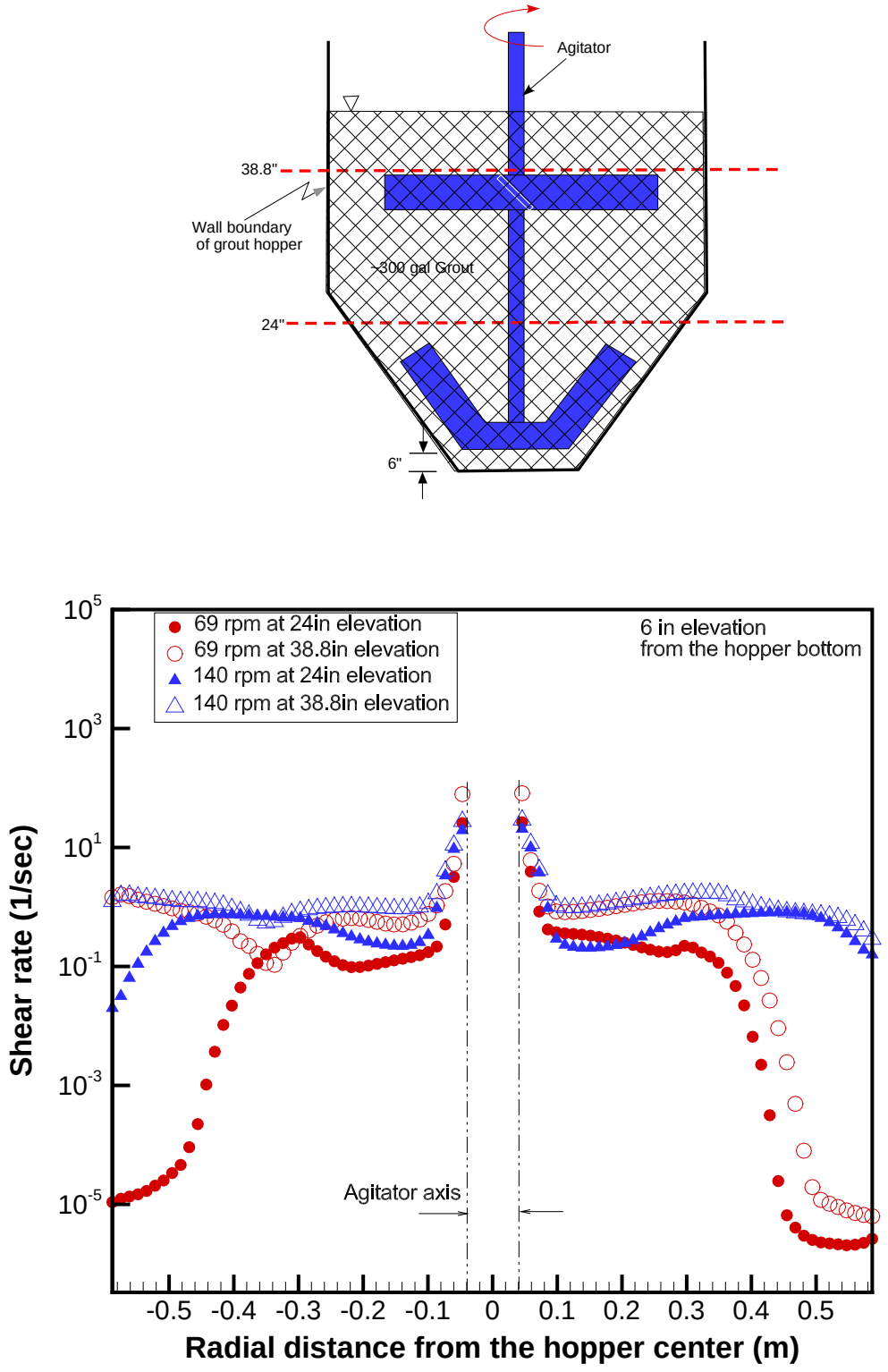

Figure 25. Comparison of grout flow shear rates for different agitator speeds at different elevations under 5 Pa yield stress

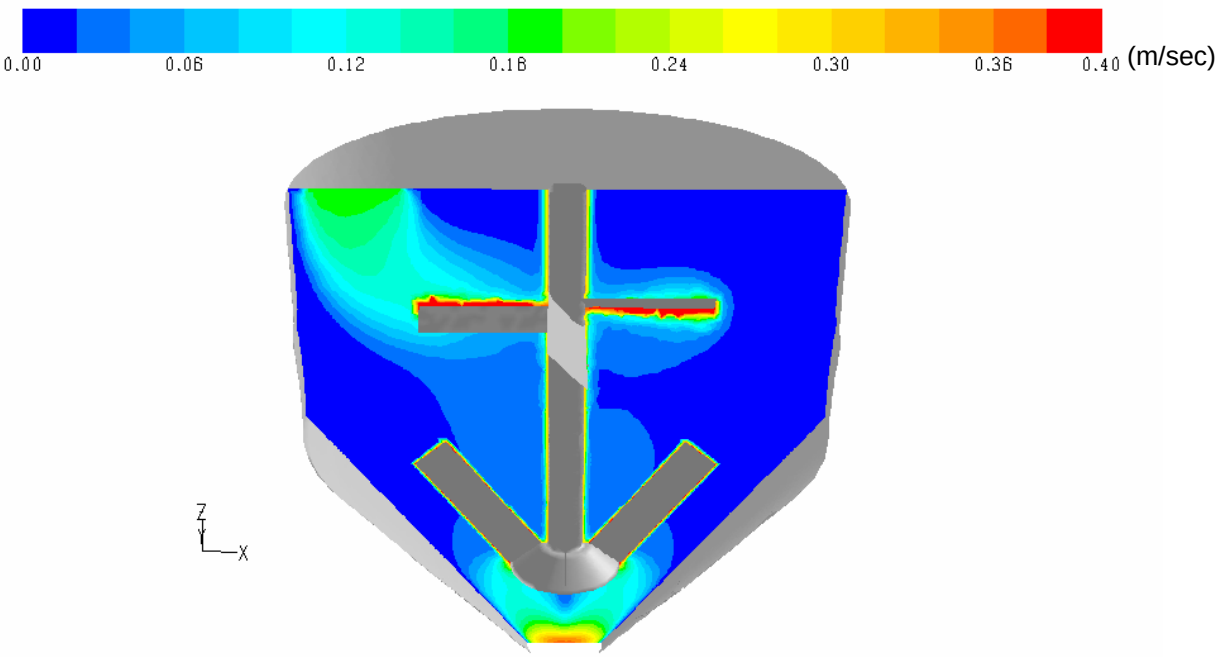

(10 in elevation from the tank bottom)

(6 in elevation from the tank bottom)

Figure 26. Comparison of velocity contour plots between two different elevations of the phase-2 agitator under 69.3 rpm

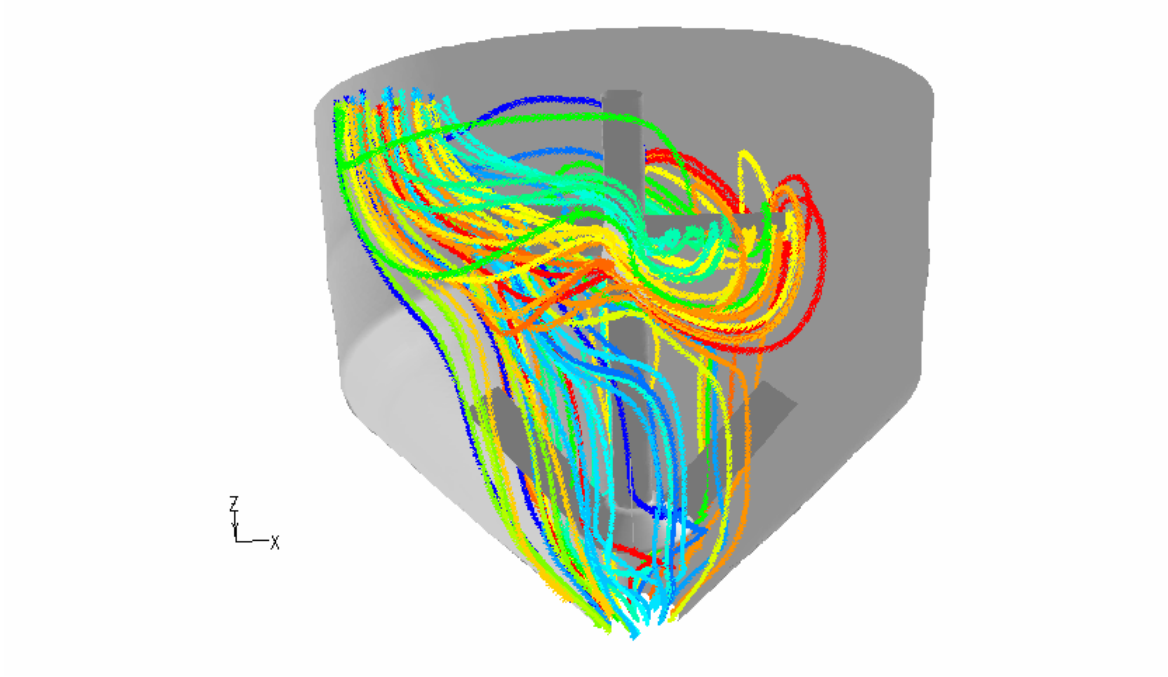

(10 in elevation from the tank bottom)

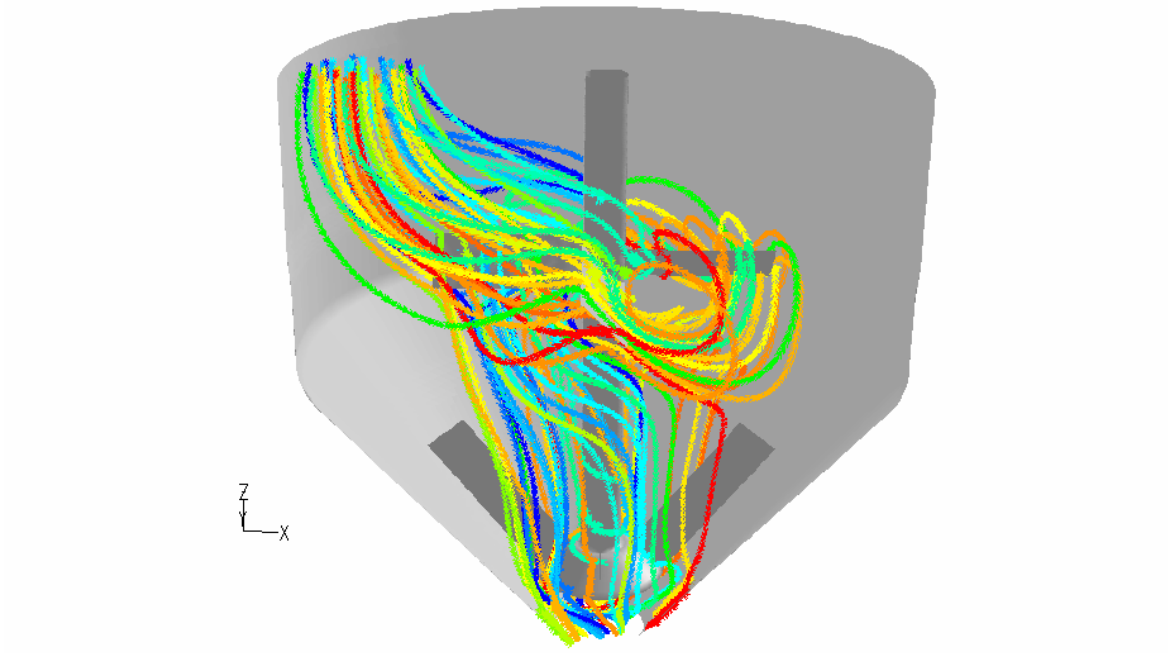

(6 in elevation from the tank bottom)

Figure 27. Comparison of primary flow path lines of the feed materials with 5 Pa yield stress between two different elevations of the phase-2 agitator under 69.3 rpm agitator speed

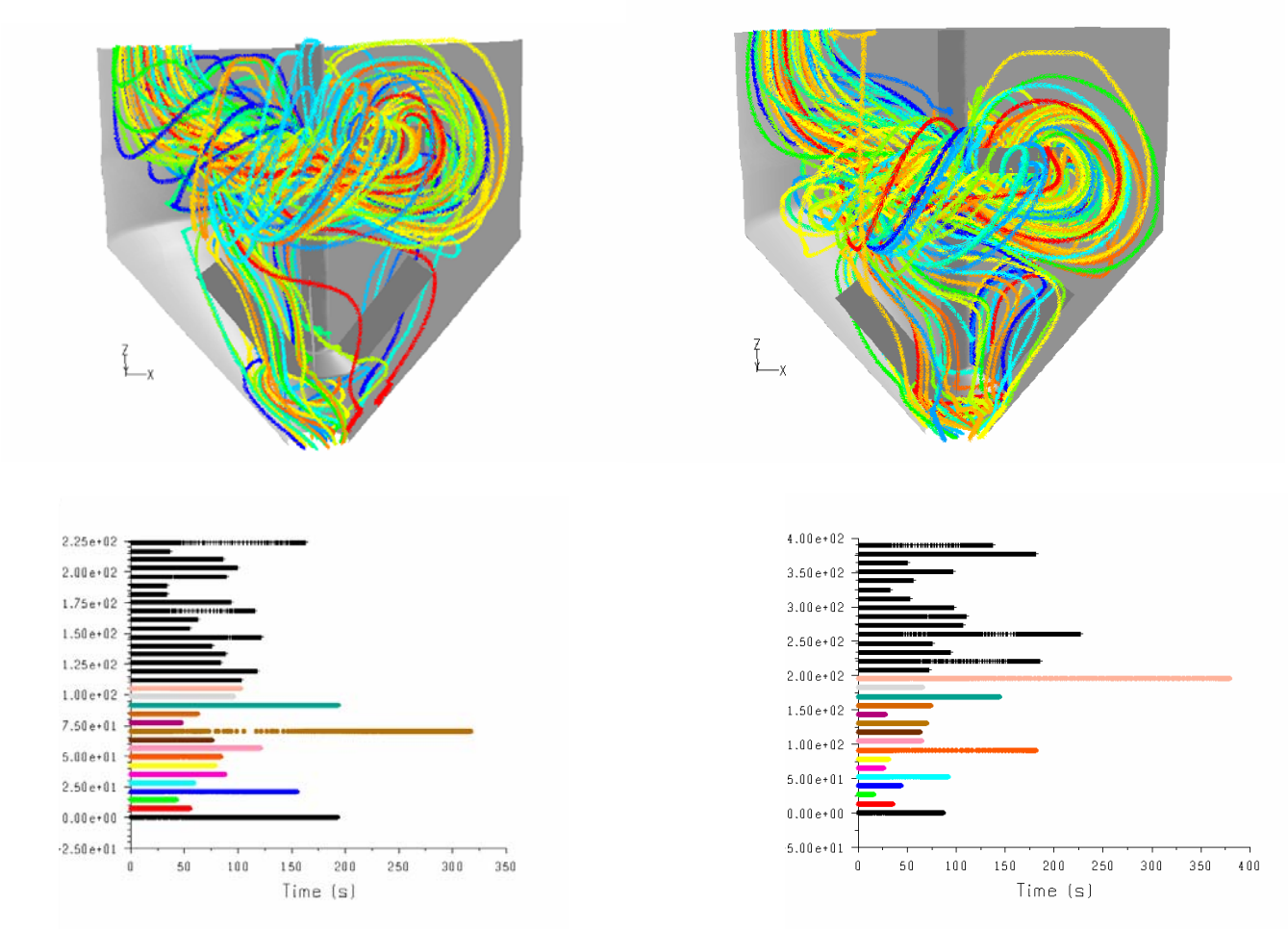

(10in dist. from the bottom, 140 rpm, turbulent flow) (6in dist. from the bottom, 140 rpm, turbulent flow)

Figure 28. Comparison of primary flow path lines and residence times of the feed materials with 5 Pa yield stress between two different elevations of the phase-2 agitator under 140 rpm agitator speed

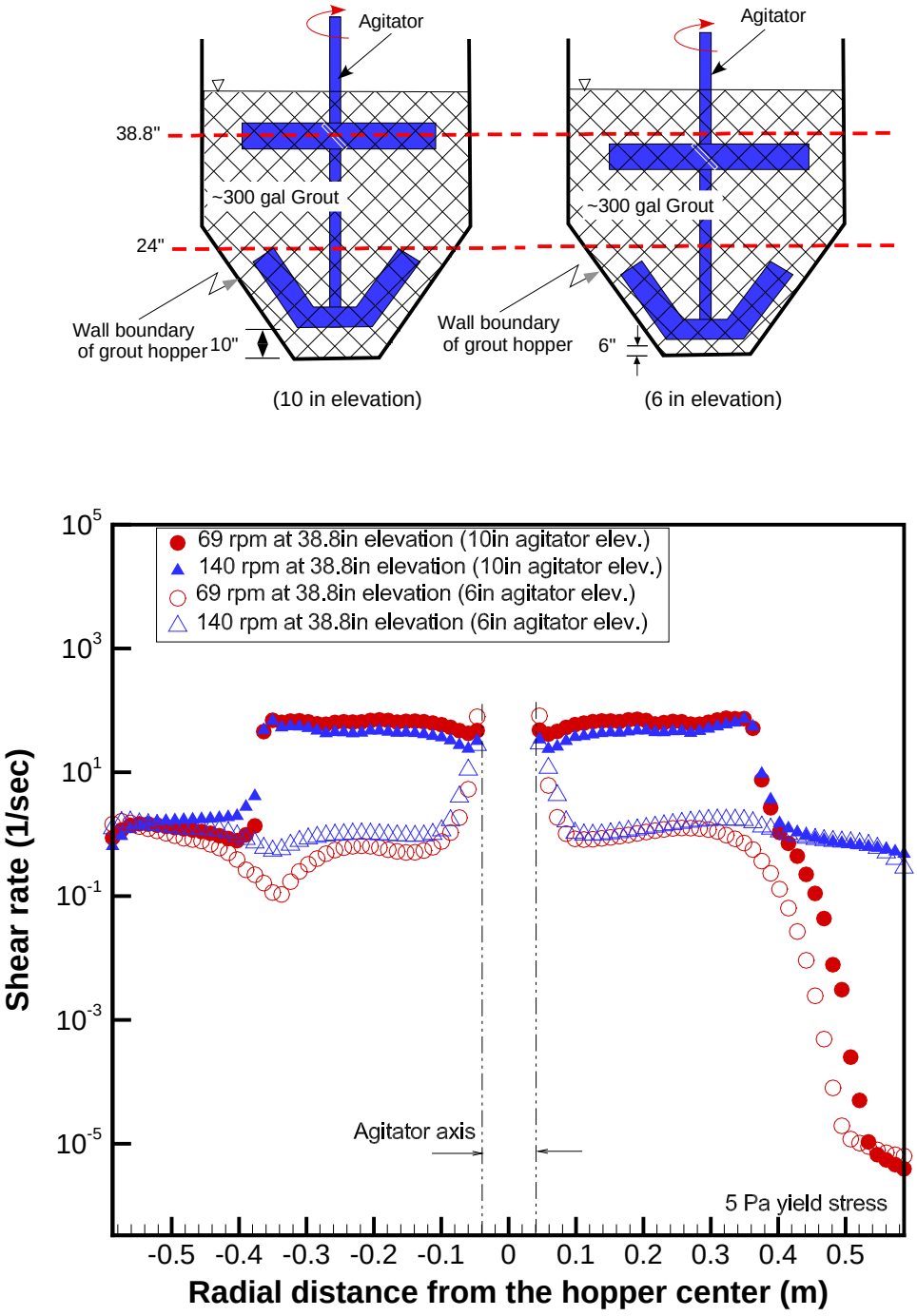

Figure 29. Comparison of shear rates of the feed materials with 5 Pa yield stress between two different elevations of the phase-2 agitator at the 39 in tank elevation height under two different agitator speeds

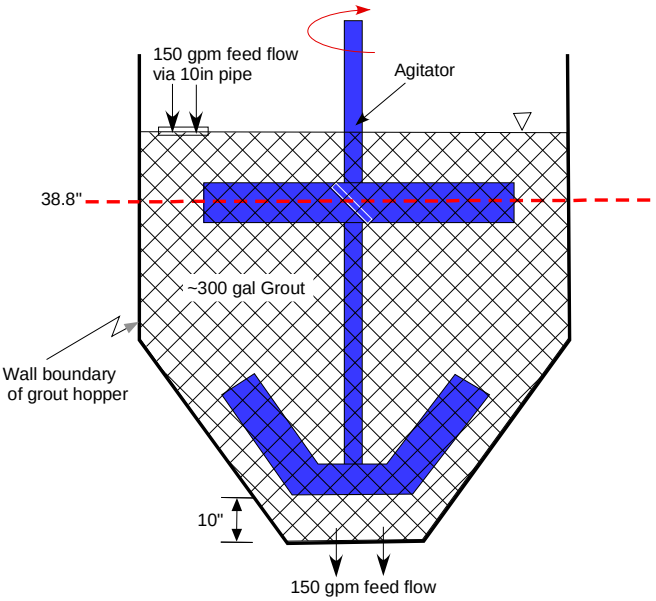

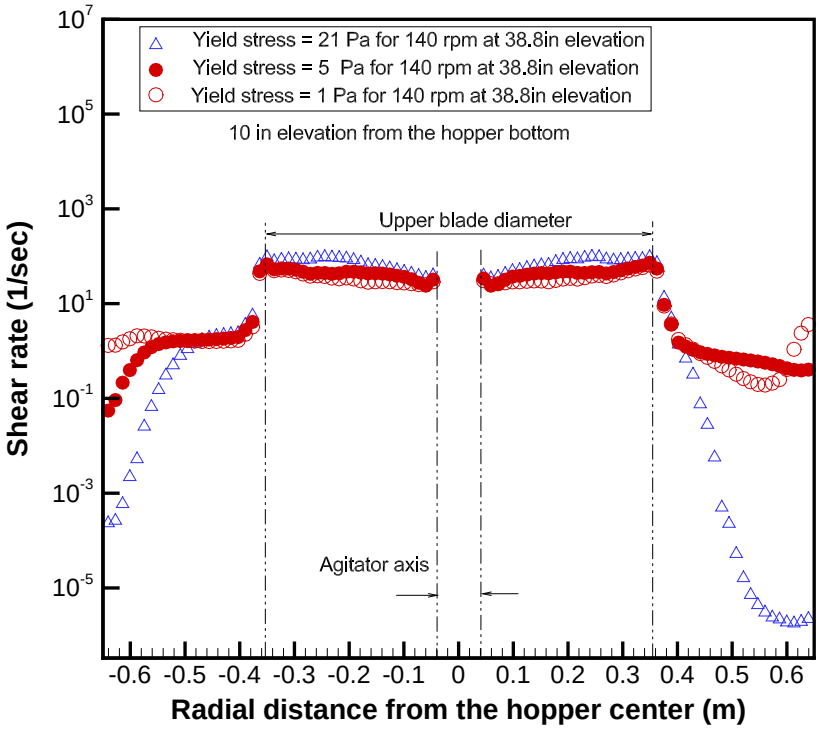

Figure 30. Comparison of shear rates along the radial distance of 38.8 in elevation for various yield stresses under 140 rpm agitator speed

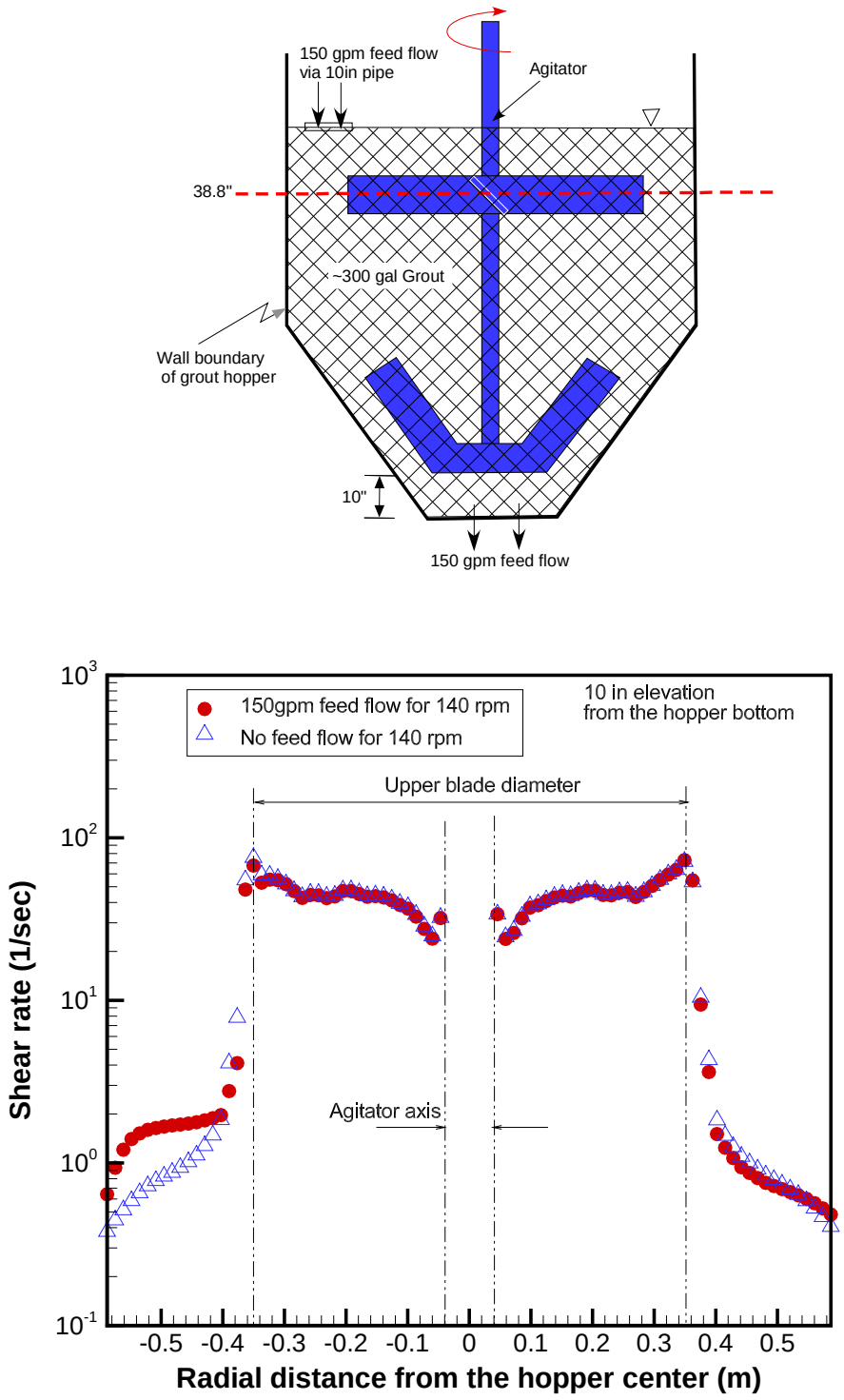

Figure 31. Comparison of shear rates along the radial distance of 38.8 in elevation for 150 gpm flow and no flow through the feed inlet under 140 rpm agitator speed with 5 Pa yield stress materials

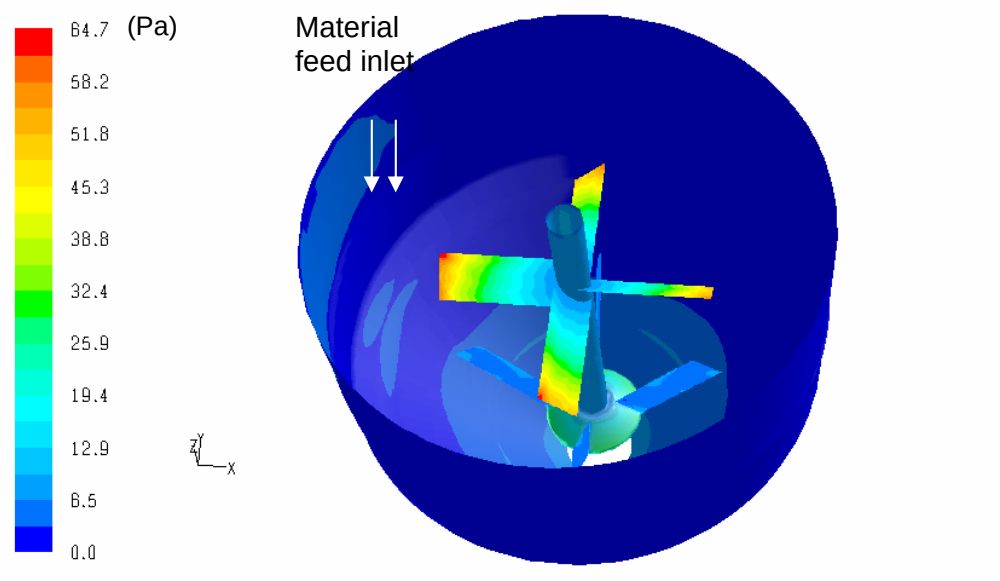

(Shear stress distributions)

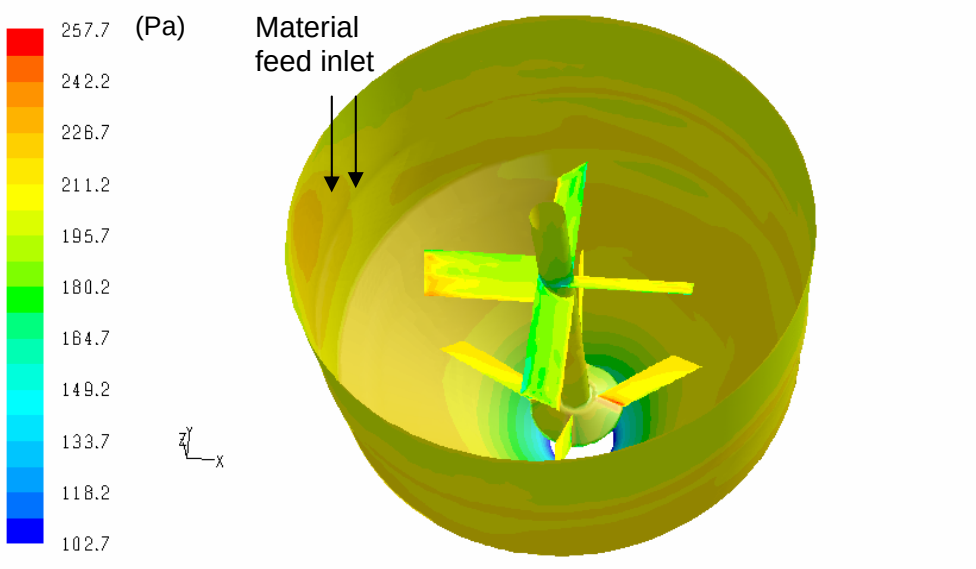

(Pressure distributions)

Figure 32. Shear stress and pressure distributions around the agitator for 150 gpm flow through the feed inlet for 69.3 rpm agitator speed with 5 Pa yield stress materials

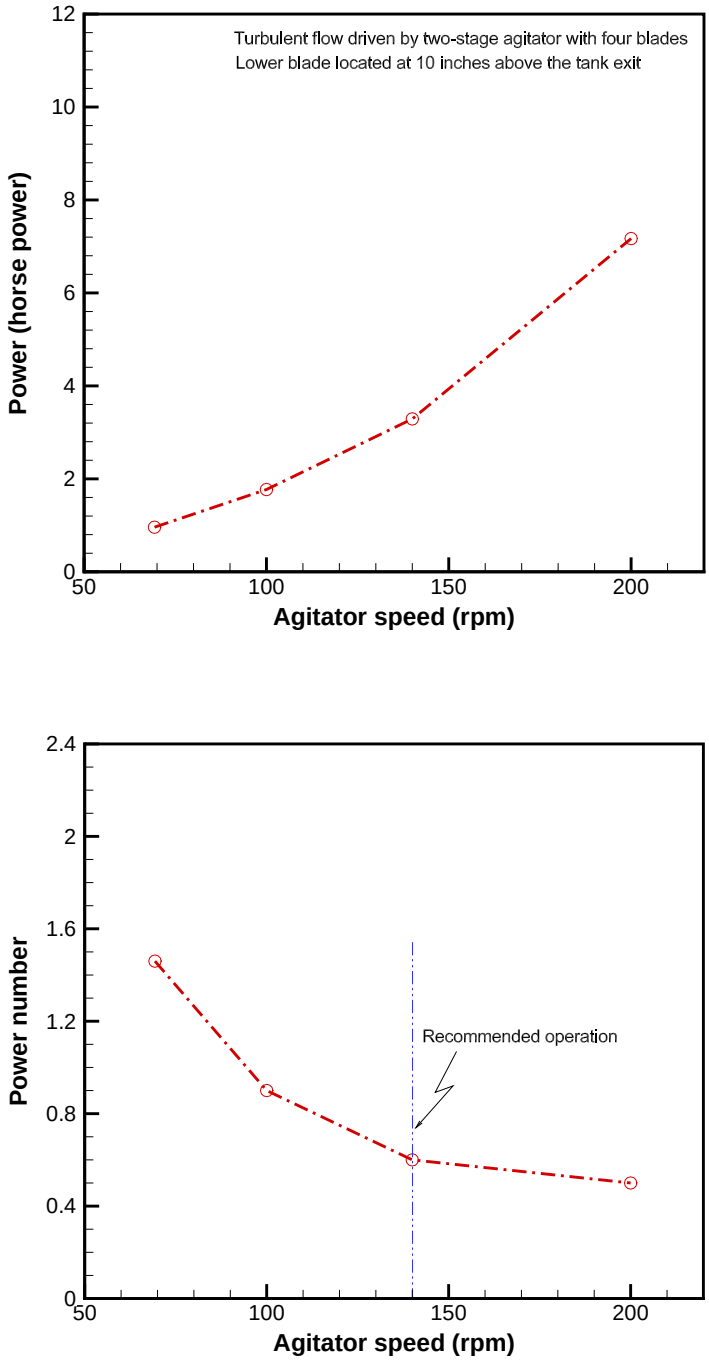

Figure 33. Power consumptions and power number for various agitator speeds for 5 Pa yield stress materials

5.0 CONCLUSIONS AND SUMMARY

A hopper tank model has been developed to evaluate the fluid stirring performance for mechanical agitators to prevent vortex pull-through and to estimate an agitator speed which provide acceptable flow performance with a 45^{o} pitched four-blade agitator. The modeling study was focused on fluid stirring, instead of traditional mixing in the literature, to keep the hopper contents such as grout in motion during its residence time. In addition, the power consumptions were estimated from the results for shear stress and pressure calculations. The results of this modeling study were used to develop the design guidelines for the agitator stirring and dispersion of the Saltstone feed materials in a hopper tank.

The modeling calculations were performed by using the two modeling steps. As a first step, a single-stage agitator with four 45^{o} pitched flat-plate propeller blades was developed for the initial phase-1 baseline analysis of the flow pattern behaviors for a range of different modeling conditions. Based on the initial phase-1 results, the phase-2 model was developed for a two-stage agitator for the improved performance calculations. The modeling results should be considered as scoping calculations since the model was not validated against test results.

A series of sensitivity calculations for different design of agitators and operating conditions have been performed to provide operational guidance for grout stirring in a 300-gallon hopper tank. In the analysis, the viscous shear was modeled by using the Bingham plastic approximation. Steady state analyses with a two-equation turbulence model were performed with the FLUENT^{TM} code. All analyses were based on three-dimensional results. Recommended operational guidance was developed assuming that local shear rates and flow patterns can be used as a measure of hydraulic performance and spatial dispersion affected by the blade passage.

The main conclusions drawn from the hopper tank modeling and calculations are as follows:

- The baseline results show that when the tank fluid has a higher yield stress, more fluid in the tank was unaffected by the blade passage and that the vortex system was not shed by the agitator blade.
- The results indicate that the mass, which flowed inside the blade, remained with the blade considerably longer than the fluid passing through the clearance area because of the wall drag.
- The flow patterns for high yield stress fluid show that there is little disturbance of the fluid in the clearance area near the wall. Thus, there is no forceable removal of material away from the tank wall boundary, which is distant from the agitated flow region.
- The phase-2 results show that when the tank fluid has a yield stress smaller than 21 Pa, more fluid in the tank was affected by the blade passage and that the vortex system was shed by the agitator blade in an efficient way.
- When the fluid is more viscous, the agitator speed has less impact on flow patterns, resulting in less vortex shedding into the stagnation zone. However, the updated two-stage agitator is much better than the single-stage baseline design in terms of flow residence time and fluid flow patterns.
- The modeling results for the phase-2 agitator design show that when the tank fluid has a turbulent flow regime, tank contents were affected by the blade passage for a wide range of yield stresses (21 to 1 Pa) and that the vortex system was shed by the agitator blade in an efficient way.

- The results show that when the phase-2 two-stage agitator is operated with the baseline speed of 69 rpm for the hopper modeling, vortex pull-through of the tank feed materials can be minimized.
- The preliminary results show that when the tank fluid has a yield stress smaller than 21 Pa, 140 rpm agitator speed is favorable in terms of flow patterns and power consumption.

6.0 REFERENCES

1. S. Y. Lee, “Grout Hopper Mixing Study”, SRNL-RP-2011-00258, Technical Task Plan, March 2011.
2. S. Y. Lee and B. W. Armstrong, “SDI CFD Modeling Analysis”, SRNL-STI-2011-00025, April 2011.
3. S. Y. Lee, R. A. Dimenna, R. A. Leishear, D. B. Stefanko, “Analysis of Turbulent Mixing Jets in a Large Scale Tank”, ASME *Journal of Fluids Engineering*, Volume 130, Number 1, pp. 011104, 2008.
4. R. A. Dimenna, S. Y. Lee , andD. A. Tamburello, “Advance Mixing Models”, SRNL-STI-2011-00026, Fubruary 2011.
5. S. Y. Lee, R. A. Dimenna, R. A. Leishear, and D. B. Stefanko, “Mixing in Large Scale Tanks Part I; Flow Modeling of Turbulent Mixing Jets”, HT-FED2004-5622, 2004 ASME Heat Transfer / Fluids Engineering Summer Conference, Charlotte, N. C., July 11-15, 2004.
6. V. E. Schrock, R. T. Revankar, R. Mannheimer, S. Y. Lee, and C-H Wang, “Critical Flow Through a Small Break on a Large Pipe with Stratified Flow”, Lawrence Berkeley National Laboratory, LBL-18386, 1985.
7. S. Y. Lee, R. A. Dimenna, J. R. Neuville, and G. A. Taylor, “Erosion Modeling Analysis For DWPF MFT/SME Tanks”, WSRC-TR-2003-00345, September 2003.
8. *FLUENT*, Fluent, Inc., 2003
9. G. B. Tatterson, *Fluid Mixing and Gas Dispersion in Agitated Tanks*, McGraw-Hill, Inc., 1991.
10. J. Baldyga and J. R. Bourne, “A Fluid Mechanical Approach To Turbulent Mixing and Chemical Reaction, Part III Computational and Experimental Results for the New Micromixing Model”, CHEM. Eng. Commun., Vol. 28, pp. 259-281, 1984.
11. W. M. Kays and M. E. Crawford, *Convective Heat and Mass Transfer*, Second Edition, McGraw-Hill Book Company, New York, 1980.
12. Hinze, J. O., *Turbulence, Second Edition*, McGraw-Hill, New York, p. 72, 1975.
13. Tennekes, H. and Lumley, J. L., *A First Course in Turbulence*, The MIT Press, Cambridge, 1972.